Signal Processing 176 (2020) 107667

Contents lists available at ScienceDirect

Signal Processing

journal homepage: www.elsevier.com/locate/sigpro

Multivariate nonlinear chirp mode decomposition

Qiming Chen [a], Lei Xie [a,*], Hongye Su [a]

State Key Laboratory of Industrial Control Technology, Zhejiang University, Hangzhou,310027 China

ARTICLE INFO

Article history:
Received 12 January 2020
Revised 12 April 2020
Accepted 24 May 2020
Available online 26 May 2020

Keywords:
Nonlinear chirp mode decomposition
Multivariate signal processing
Multivariate variational mode decomposition
Time-frequency analysis

ABSTRACT

In this paper, a novel Multivariate Nonlinear Chirp Mode Decomposition (MNCMD) is proposed. In contrast to most existing multivariate time-frequency decomposition approaches, the proposed MNCMD is capable of handling *time-varying* signal efficiently in an elegant variational optimization framework. The multivariate nonlinear chirp mode is defined based on the presence of a joint or common instantaneous frequency component among all channels of input signal. Then the objective function of MNCMD is defined as the sum of mode bandwidths across all signal channels. The alternate direction method of multipliers (ADMM) algorithm is employed to optimize the MNCMD problem. MNCMD can extract an optimal set of multivariate modes and their corresponding instantaneous frequencies without requiring more user-defined parameters than the original NCMD. The effectiveness and advantages of the proposed MNCMD are demonstrated by studying its mode-alignment, filter bank structure, quasi-orthogonality, the influence of channel number, noise robustness, and convergence. Specifically, we highlight the utility and superiority of the proposed method in three real-world applications, including the analysis of an oceanographic float position record (two-channel), the separation of α-rhythms in electroencephalogram (EEG) data (four-channel), and the detection of plant-wide oscillations in industrial control systems (nine-channel).

1. Introduction

Many common data, such as those sampled from nature, human-beings, and industrial systems, contain valuable information [1]. Generally, these data show nonlinear and nonstationary characteristics and are called nonlinear chirp signals (NCSs) [2]. It is a challenging task to analyze them directly. The primary goal of signal processing is to reveal these underlying information and structures.

1.1. Univariate signal processing

The traditional methods focus on signal transformation. For example, Fourier Transform (FT) enables us to analyze signals from frequency domain. Fourier-based analysis rules over linear time invariant and stationary signal processing. However, due to fixed and global basis functions, it only provides global frequency information and thus lacks ability of characterizing time-varying frequency contents of NCSs. In order to obtain the time-frequency (T-F) information of signals, it is necessary to change the way of global transformation to local transformation. Gabor [3] presented the short-time Fourier transform (STFT) to perform the joint analysis of time and frequency. But it cannot automatically adjust time window and frequency window. Cohen [4] developed an unified representation of time-frequency distribution, and the most important one is Wigner-Ville distribution (WVD). Nevertheless, its T-F spectrum is spoiled by the cross-term interference. Wavelet transform (WT) [5] was then established based on scale and time-shift joint analysis and it became a powerful signal processing tool. Nevertheless, the success of WT heavily depends on the manual selection of decomposition levels and the mother wavelet.

Based on basis function expansion, the above traditional methods have the advantages of simplicity, uniqueness and symmetry, but they lack flexibility and are not adaptive amenable enough for complex signal analysis. Starting from empirical mode decomposition (EMD) [6], data-driven signal decomposition and T-F techniques have become a research hotspot. They can act without a prior on input data. Fig. 1 briefly summarizes the development of the related approaches and the proposed method. A brief overview is provided as follows.

EMD can adaptively extract a set of oscillatory modes by signal extrema and sifting process [6]. This method is not restricted by Heisenberg uncertainty principle but lacks mathematical foundation, and it is sensitive to noise and sampling. In order to remedy EMD's limitations, some modified versions are developed in succession, such as ensemble EMD (EEMD) [7] and complementary EEMD (CEEMD) [8]. In addition, some algorithms similar

* Corresponding author. Fax: 8657187951200.
E-mail address: leix@iipc.zju.edu.cn (L. Xie).

https://doi.org/10.1016/j.sigpro.2020.107667
0165-1684/

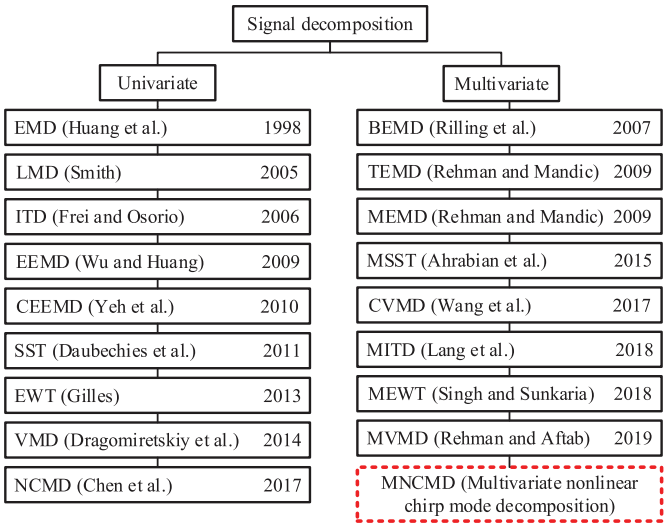

Fig. 1. A brief list of signal decomposition methods. MNCMD is the proposed method in this paper; it is shown in the red dash box. (For interpretation of the references to colour in this figure legend, the reader is referred to the web version of this article.)

to EMD are also proposed. For example, Smith [9] raised local mean decomposition (LMD) method through separating amplitude-modulation (AM) and frequency-modulation (FM). Frei and Osorio [10] put forward intrinsic time-scale decomposition (ITD) with low computational complexity. However, these methods suffer problems similar to EMD, including but not limited to mode-mixing and end-effect. Unlike the above EMD-based decomposition scheme, some methods retrieve the mode information from proper time-frequency distributions. For instance, synchrosqueezed transform (SST) [11] utilized a reassignment operator to search the T-F coefficients of each mode and then reconstruct the modes using inverse T-F transforms. Nevertheless, SST requires the modes are well separated in the T-F plane. Empirical wavelet transform (EWT) [12] combined the wavelet filter bank and adaptive local iterative filtering method to extract signal modes. However, its performance relies on the support detection algorithm.

Recently, Dragomiretskiy and Zosso [13] proposed the variational mode decomposition (VMD) algorithm that is based on convex optimization theory. They formulated an optimization objective function with the assumption that the most compact mode is found around a center frequency ω_k. In VMD, the mode bandwidth is estimated as H^1 Gaussian smoothness of the corresponding baseband signal, which is shifted from its analytic signal via harmonic mixing. VMD's idea is very innovative and creative and has attractive performance in several aspects, such as robustness and anti-mode-mixing [14]. However, the center frequency is estimated as the center-of-gravity of the mode's power spectrum. Therefore, VMD is not proper to process time-varying signals. In addition, VMD is still formulated in the frequency domain, thus it cannot provide time-frequency information. More recently, inspired by VMD and sparsification approach [15,16], Chen et al. [2] proposed a nonlinear chirp mode decomposition (NCMD) algorithm, which was also a variational method and could analyze time-varying NCSs. It mainly utilized the demodulation techniques to transform a time-varying NCS into a narrow-band signal. Specifically, for each mode (nonlinear chirp mode, NCM), two demodulated quadrature signals can be iteratively updated by two time-frequency filters with the current estimated IF; then based on the phase information provided by the two quadrature signals, the IF can be further updated by the arctangent demodulation technique. The solution of NCMD could be obtained by repeating the above two steps until the bandwidth of the demodulated signal is the narrowest [17]. NCMD is capable of accurately extracting the instantaneous frequencies (IFs) and instantaneous amplitudes (IAs) of signals with very close or even crossed modes.

1.2. Multivariate signal processing

With the development of computers and sensors, multivariate signal processing techniques are widely demanded and applied in various fields [18], such as disease diagnosis [19,20] and denoising [21]. Generally, multivariate signal decomposition and T-F analysis involve two main requirements [1]: (i) mode-alignment, namely, the alignment of common or joint oscillations (with similar frequency information) across multiple channels of each mode; (ii) extracting any correlation between multiple data channels. There has been a surge of interest in extending existing univariate methods to process multivariate (multichannel) signals [1,22]

The most straightforward methods for multivariate signal processing is analyzing each channel of a multivariate signal separately using univariate signal processing techniques. In this way, the results would not fulfill the above requirements, because the mutual relationships among channels are not considered.

In recent years, advances in signal acquisition tools have highlighted the demanding for synchronous processing of multichannel data [23]. Therefore, it is necessary to develop specialized extensions for multivariate data that operate directly in multidimensional space where signal resides. The univariate EMD has been extended to various versions including those suitable for the bivariate [24], trivariate [25], and multivariate [26] signals. The first two methods can be considered as subsets of the last one. Multivariate EMD (MEMD) works on the principle of separating faster multivariate oscillations from slower ones. It has been applied to various fields, such as image fusion [27], process control [28], and biomedical engineering [29]. However, apart from inheriting the drawbacks of the univariate EMD, such as sensitivity to sampling and noise, the performance of MEMD also relies on the selection of projection number and directions.

Later, based on similar extension method, Lang et al. proposed two kinds of multivariate ITD (MITD) algorithms, namely, indirect MITD (IMITD) [30] and direct MITD (DMITD) [31]. Nevertheless, these MITD methods are also subjected to limitations of univariate ITD. Recently, multivariate SST (MSST) [32] and multivariate EWT (MEWT) [33] have also been reported. They are wavelet-based approaches. However, MSST only provides a graphical representation of T-F spectrum and lacks mode separation ability. MEWT is simplistic but relies on predefined boundaries of wavelet filterbank, which is a tricky problem in practice. VMD-based multivariate signal processing methods, including complex VMD (CVMD) [34] and multivariate VMD (MVMD) [1], are novel and attractive. Actually, CVMD is different from the latter since it cleverly uses the original VMD to decompose bivariate time series based on properties of the complex field, thus it cannot be extended to the cases with more than two variables. MVMD first defines a multivariate oscillations using analytic signal representation based on Hilbert transform with a constraint that a joint frequency component exists among all signal channels. Then it established a multivariate variational model as a generic extension of univariate VMD. MVMD not only inherits properties of VMD, but also shows mode-alignment and quasi-orthogonality. It is the most promising development in multivariate signal decomposition. However, because MVMD's center frequency is estimated as the center-of-gravity of the mode's power spectrum, it is not proper to process time-varying signals. In addition, MVMD cannot provide T-F information intuitively.

As discussed above, most existing methods are limited to process narrow-band signals and there is a lack of techniques for time-varying multivariate signal decomposition. To tackle this is-

sue, this paper proposes a multivariate nonlinear chirp mode decomposition (MNCMD) algorithm. In the presented variational model of MNCMD, we first define a multivariate nonlinear chirp mode (MNCM) based on the instantaneous frequency information among all channels of input data. Derived from the fact that a time-varying MNCM can be transformed into a narrow-band multivariate signal through demodulation techniques, an objective function is then established based on minimizing the sum of bandwidths of the modes across all signal channels. Minimization of the MNCMD model can be effectively achieved through the alternate direction method of multipliers (ADMM). As a genetic extension of univariate NCMD model to multivariate signals, the proposed MNCMD inherits a lot of desirable properties of univariate NCMD. And it can extract an optimal set of multivariate modes and their corresponding instantaneous frequencies without requiring more user-defined parameters than the original NCMD. The effectiveness and advantages of MNCMD is demonstrated by extensive simulated and real-world signals. We specifically focus on investigating its mode-alignment property, filter bank structure, quasi-orthogonality, influence of channel number, noise robustness, and convergence.

The development of the proposed MNCMD scheme will be detailed in the following sections. Section 2 introduces the univariate NCMD. The proposed MNCMD is described elaborately in Section 3. The study on the properties of MNCMD is given in Section 4, including mode-alignment, filter bank structure, quasi-orthogonality, influence of channel number, noise robustness, and convergence. In Section 5, real-world applications in three fields, including the analysis of an oceanographic float position record (two-channel), the separation of α-rhythms in EEG data (four-channel), and the detection of plant-wide oscillations in industrial control systems (nine-channel), are provided to validate the effectiveness and advantages of the proposed methodology. These are followed by conclusions in Section 6.

2. Nonlinear chirp mode decomposition

Nonlinear chirp modes (NCMs) are AM-FM (amplitude-modulated and frequency-modulated) functions, which can be given by

$$g(t) = a(t)\cos\left(2\pi\int_0^t f(s)ds + \phi\right) \tag{1}$$

where $a(t)$, $f(t) > 0$ are the instantaneous amplitude (IA) and the instantaneous frequency (IF), respectively. ϕ stands for the initial phase. Generally, IA and IF are assumed to be smooth functions. Note that, for notational simplicity, the subscript i is omitted in (1). In practice, the nonstationary signal $x(t)$, called as NCS, usually does not satisfy the conditions of Hilbert transform [13]. That is to say, it is infeasible to conduct time-frequency analysis of $x(t)$ directly. To tackle this issue, NCMD assumes a NCS is composed of Q NCMs [2], which meet the above conditions. Thus the nonstationary signal $x(t)$ can be expressed as the sum of multiple NCMs, as shown in (2).

$$\begin{aligned} x(t) &= \sum_{i=1}^{Q} g_i(t) + \eta(t) \\ &= \sum_{i=1}^{Q} a_i(t)\cos\left(2\pi\int_0^t f_i(s)ds + \phi_i\right) + \eta(t) \end{aligned} \tag{2}$$

where $\eta(t) \sim \mathcal{N}(0, \sigma^2)$ is the white Gaussian noise. When $x(t)$ is decomposed into a set of NCMs $g_i(t)$, the corresponding analytic signals $g_{i,A}(t)$ are generated by Hilbert transform

$$\begin{aligned} g_{i,A}(t) &= g_i(t) + \mathcal{H}(g_i(t)) \\ &= a_i(t)\exp\left(2\pi\int_0^t f_i(s)ds + \phi_i\right) \end{aligned} \tag{3}$$

where $\mathcal{H}(\cdot)$ stands for the Hilbert transform. Then the IFs can be obtained by phase demodulation [2,13].

The NCS model (2) can be rewritten into a demodulated form as

$$\begin{aligned} x(t) = \sum_{i=1}^{Q} & \underbrace{a_i(t)\cos\left(2\pi\int_0^t \left(f_i(s) - \tilde{f}_i(s)\right)ds + \phi_i\right)}_{u_i(t)} \\ & \times \cos\left(2\pi\int_0^t \tilde{f}_i(s)ds\right) \\ & \underbrace{-a_i(t)\sin\left(2\pi\int_0^t \left(f_i(s) - \tilde{f}(s)\right)ds + \phi_i\right)}_{v_i(t)} \\ & \times \sin\left(2\pi\int_0^t \tilde{f}_i(s)ds\right) + \eta(t) \\ = \sum_{i=1}^{Q} & u_i(t)\cos\left(2\pi\int_0^t \tilde{f}_i(s)ds\right) + v_i(t) \\ & \times \sin\left(2\pi\int_0^t \tilde{f}_i(s)ds\right) + \eta(t) \end{aligned} \tag{4}$$

where $u_i(t)$ and $v_i(t)$ represent two demodulated signals; IA could be reconstructed as $a_i = \sqrt{(u_i(t))^2 + (v_i(t))^2}$; $\tilde{f}_i(s)$ stands for the frequency function of demodulation operator. According to the basic idea of the NCMD that the demodulated signals $u_i(t)$ and $v_i(t)$ will have the narrowest frequency band when $f_i(s) = \tilde{f}_i(s)$, the decomposition problem can be formulated as

$$\begin{aligned} &\min_{\{u_i(t)\},\{v_i(t)\},\{\tilde{f}_i(t)\}} \left\{\sum_{i=1}^{Q} \left\|u_i''(t)\right\|_2^2 + \left\|v_i''(t)\right\|_2^2\right\} \\ &s.t. \left\| x(t) - \sum_{i=1}^{Q} u_i(t)\cos\left(2\pi\int_0^t \tilde{f}_i(s)ds\right) \right. \\ &\left. + v_i(t)\sin\left(2\pi\int_0^t \tilde{f}_i(s)ds\right)\right\|_2 \le \varepsilon \end{aligned} \tag{5}$$

where the square of the l_2 norm of the second-order derivative is used to estimate the signal bandwidth [35]; $\varepsilon > 0$ is an upper bound determined by the noise level. Then, the augmented Lagrangian multiplier and ADMM (alternate direction method of multipliers) are adopted to solve (5). The details of the optimization procedures are available in [2].

3. Multivariate nonlinear chirp mode decomposition

3.1. Multivariate nonlinear chirp mode

In order to develop a multivariate version of NCMD, we need to define an multivariate nonlinear chirp mode (MNCM). Firstly, a set of multivariate AM-FM signals with M channels can be represented in a vector form [36]

$$\mathbf{g}(t) = \begin{bmatrix} g_1(t) \\ g_2(t) \\ \vdots \\ g_M(t) \end{bmatrix} = \begin{bmatrix} a_1(t)\cos\left(2\pi\int_0^t f_1(s)ds + \phi_1\right) \\ a_2(t)\cos\left(2\pi\int_0^t f_2(s)ds + \phi_2\right) \\ \vdots \\ a_M(t)\cos\left(2\pi\int_0^t f_M(s)ds + \phi_M\right) \end{bmatrix} \tag{6}$$

where $a_m(t)$, f_m, and ϕ_m denote the IA, IF and initial phase for the m-th component respectively. Then, the corresponding analytic representation of the vector signal $\boldsymbol{g}(t)$ is given by

$$\begin{aligned}\boldsymbol{g}_A(t) &= \boldsymbol{g}(t) + j\mathcal{H}(\boldsymbol{g}(t)) \\ = \begin{bmatrix} g_A^1(t) \\ g_A^2(t) \\ \vdots \\ g_A^M(t) \end{bmatrix} &= \begin{bmatrix} a_1(t)\exp\left(j\left(2\pi\int_0^t f_1(s)ds + \phi_1\right)\right) \\ a_2(t)\exp\left(j\left(2\pi\int_0^t f_2(s)ds + \phi_2\right)\right) \\ \vdots \\ a_M(t)\exp\left(j\left(2\pi\int_0^t f_M(s)ds + \phi_M\right)\right) \end{bmatrix}.\end{aligned} \tag{7}$$

where $\mathcal{H}$ represents the Hilbert transform. It is notable that the mathematical description of (7) regards the M channel in isolation from each other. For a multivariate nonlinear chirp mode, there may be one or more common frequency components contain in $\boldsymbol{g}(t)$. Herein, we adopt a simplified multivariate analytic signal expression for $\boldsymbol{g}_A(t)$ that requires a single common component among all channels [2,36], namely,

$$\begin{aligned}\boldsymbol{g}_A(t) &= \begin{bmatrix} a_1(t) \\ a_2(t) \\ \vdots \\ a_M(t) \end{bmatrix} \exp\left(j\left(2\pi\int_0^t f(s)ds + \phi\right)\right) \\ &= \boldsymbol{a}(t)\exp\left(j\left(2\pi\int_0^t f(s)ds + \phi\right)\right).\end{aligned} \tag{8}$$

Model (8) is the analytic form of MNCM and will be used to formulate the objective function of MNCMD algorithm in the following section.

3.2. Objective function

Because the demodulation only involves the phase part of a time-varying NCM, we can use the technology similar to the univariate NCM demodulation to demodulate the multivariate NCM. Herein, a demodulation operator (DO) Φ^- [2,37] is given by

$$\Phi^-(t) = \exp\left(-j2\pi\left(\int_0^t f_d(s)ds - f_c t\right)\right) \tag{9}$$

where f_d typifies the frequency function of the operator; f_c is carrier frequency. The corresponding demodulated MNCM $\boldsymbol{g}_A^d(t)$ is calculated by multiplying $\boldsymbol{g}_A(t)$ with the demodulation operator Φ^-:

$$\begin{aligned}\boldsymbol{g}_A^d(t) &= \boldsymbol{g}_A(t)\Phi^-(t) \\ &= \boldsymbol{a}(t)\exp\left(j2\pi\int_0^t f(s) - f_d(s)ds + j\phi + j2\pi f_c t\right).\end{aligned} \tag{10}$$

When the frequency function of DO f_d is matched to that of MNCM (i.e., $f(s) = f_d(s)$), $\boldsymbol{g}_A^d(t)$ would be a purely AM signal centered around the carrier frequency f_c. That is to say, the demodulated MNCM will have the narrowest band, which is consistent with the conclusions in univariate case [38,39].

It can be observed from Fig. 2 that the demodulated signal indeed has a more compact spectrum.

After demodulation, in order to measure the bandwidth of a AM signal, it is necessary to move the mode's spectrum to "baseband" by mixing demodulated signal with a frequency-shift operator $\exp(-j2\pi f_c t)$, namely, the multivariate baseband signal is given by

$$\boldsymbol{g}_A^b(t) = \boldsymbol{g}_A^d(t)\exp(-j2\pi f_c t). \tag{11}$$

The spectrum of the baseband signal is shown in the right graph of Fig. 2. It is apparent that the baseband mode is a zero intermediate frequency signal and the frequency-shift operator does not change the bandwidth of $\boldsymbol{g}_A^d(t)$. It is worth noting that the operations of (10) and (11) can be combined as

$$\boldsymbol{g}_A^b(t) = \boldsymbol{g}_A(t)\exp\left(-j2\pi\int_0^t f(s)ds\right) \tag{12}$$

where $f(t)$ is the IF of the original MNCM. Therefore, our approach is estimating the IF of a MNCM by searching a smooth function $\tilde{f}(s)$ with which the resulting baseband signal has the narrowest band. It should be noted that MVMD only involves the frequency-shift operation without demodulation, which means MVMD cannot extract the IF information and process time-varying signals.

In the end, the MNCM can be recovered using trigonometric identity, given by

$$\begin{aligned}\boldsymbol{g}(t) &= \mathrm{Re}\{\boldsymbol{g}_A(t)\} \\ &= \mathrm{Re}\left\{\boldsymbol{g}_A^b(t)\exp\left(j2\pi\int_0^t \tilde{f}(s)ds\right)\right\} \\ &= \mathrm{Re}\left\{\boldsymbol{g}_A^b(t)\right\}\cdot\mathrm{Re}\left\{\exp\left(j2\pi\int_0^t \tilde{f}(s)ds\right)\right\} \\ &\quad - \mathrm{Im}\left\{\boldsymbol{g}_A^b(t)\right\}\cdot\mathrm{Im}\left\{\exp\left(j2\pi\int_0^t \tilde{f}(s)ds\right)\right\} \\ &= \boldsymbol{u}(t)\cos\left(2\pi\int_0^t \tilde{f}(s)ds\right) + \boldsymbol{v}(t)\sin\left(2\pi\int_0^t \tilde{f}(s)ds\right)\end{aligned} \tag{13}$$

where $\boldsymbol{u}(t)$ and $\boldsymbol{v}(t)$ are two demodulated signals expressed as

$$\boldsymbol{u}(t) = \boldsymbol{a}(t)\cos\left(2\pi\int_0^t \left(f(s) - \tilde{f}(s)\right)ds + j\phi\right) \tag{14}$$

$$\boldsymbol{v}(t) = -\boldsymbol{a}(t)\sin\left(2\pi\int_0^t \left(f(s) - \tilde{f}(s)\right)ds + j\phi\right). \tag{15}$$

Assuming the mode number and channel number are Q and M, respectively, then the multivariate input data $\boldsymbol{X} = [\ x_1 \quad x_2 \quad \dots \quad x_M\ ]^T$ can be written as

$$\begin{aligned}\boldsymbol{X}(t) &= \sum_{i=1}^{Q}\boldsymbol{g}_i(t) = \sum_{i=1}^{Q}\boldsymbol{u}_i(t)\cos\left(2\pi\int_0^t \tilde{f}_i(s)ds\right) \\ &\quad + \boldsymbol{v}_i(t)\sin\left(2\pi\int_0^t \tilde{f}_i(s)ds\right) + \eta(t) \\ &= \sum_{i=1}^{Q}\begin{bmatrix} u_{i,1}(t) \\ u_{i,2}(t) \\ \vdots \\ u_{i,M}(t) \end{bmatrix}\cos\left(2\pi\int_0^t \tilde{f}_i(s)ds\right) \\ &\quad + \begin{bmatrix} v_{i,1}(t) \\ v_{i,2}(t) \\ \vdots \\ v_{i,M}(t) \end{bmatrix}\sin\left(2\pi\int_0^t \tilde{f}_i(s)ds\right) + \eta(t).\end{aligned} \tag{16}$$

The goal of MNCMD is to extract an ensemble of multivariate nonlinear chirp modes from the multivariate input data such that the sum of bandwidth of the extracted modes is minimum. To this end, the resulting objective function of the MNCMD then becomes a multivariate extension of that used in the univariate NCMD (5) and is formulated as

$$\begin{aligned}&\min_{\{u_i^m(t)\},\{v_i^m(t)\},\{\tilde{f}_i(t)\}} \sum_{i=1}^{Q}\sum_{m=1}^{M}\left\{\left\|u''_{i,m}(t)\right\|_2^2 + \left\|v''_{i,m}(t)\right\|_2^2\right\} \\ &s.t.\left\|x_m(t) - \sum_{i=1}^{Q}u_{i,m}(t)\cos\left(2\pi\int_0^t \tilde{f}_i(s)ds\right)\right. \\ &\left. + v_{i,m}(t)\sin\left(2\pi\int_0^t \tilde{f}(s)ds\right)\right\|_2 \le \varepsilon_m,\ m = 1, 2, \dots, M.\end{aligned} \tag{17}$$

To avoid confusion, the subscript i and m represent mode index and channel index, respectively.

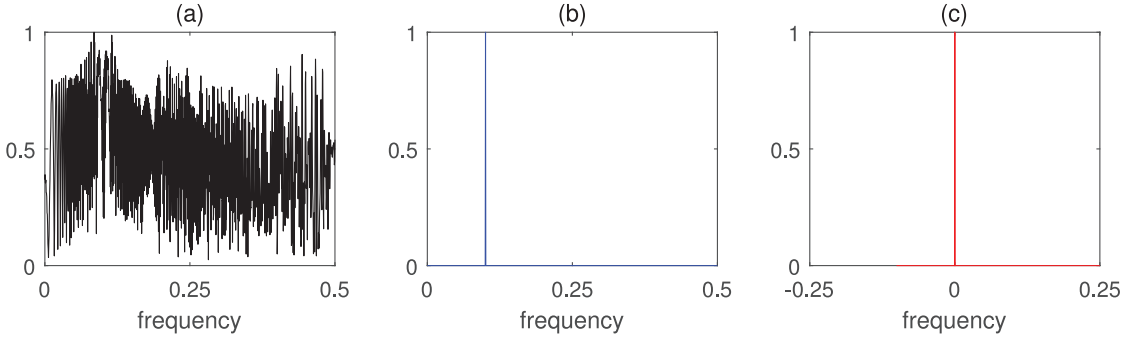

Fig. 2. (a) spectrum of a time-varying signal; (b) spectrum of the corresponding demodulated signal; and (c) spectrum of the corresponding baseband signal.

3.3. Algorithm

Because signals are discrete points in practice, model (17) is discretized in this section. Assuming that the signals are sampled at $t = t_0, \ldots, t_{N-1}$, the discrete form of (17) is

$$\min_{\{\boldsymbol{u}_{i,m}\},\{\boldsymbol{v}_{i,m}\},\{\boldsymbol{f}_i\}} \left\{ \sum_{i=1}^{Q}\sum_{m=1}^{M} \left(\|\Omega \boldsymbol{u}_{i,m}\|_2^2 + \|\Omega \boldsymbol{v}_{i,m}\|_2^2 \right) \right\}$$
$$s.t. \left\| \boldsymbol{x}_m - \sum_{i=1}^{Q} (\boldsymbol{A}_i \boldsymbol{u}_{i,m} + \boldsymbol{B}_i \boldsymbol{v}_{i,m}) \right\|_2 \le \varepsilon_m, m = 1, 2, \ldots, M \tag{18}$$

where $\boldsymbol{u}_{i,m} = [u_{i,m}(t_0), \ldots, u_{i,m}(t_{N-1})]^T$, $\boldsymbol{v}_{i,m} = [v_{i,m}(t_0), \ldots, v_{i,m}(t_{N-1})]^T$, $\boldsymbol{f}_i = [\tilde{f}_i(t_0), \ldots, \tilde{f}_i(t_{N-1})]^T$, $\boldsymbol{x}_m = [x_m(t_0), \ldots, x_m(t_{N-1})]^T$, $\varphi_i(t) = 2\pi \int_0^t \tilde{f}_i(s)ds$, $\boldsymbol{A}_i = diag[\cos(\varphi_i(t_0)), \ldots \cos(\varphi_i(t_{N-1}))]$, $\boldsymbol{B}_i = diag[\sin(\varphi_i(t_0)), \ldots \sin(\varphi_i(t_{N-1}))]$, and Ω is a second-order difference operator [2] given as

$$\Omega = \begin{bmatrix} -1 & 1 & 0 & \cdots & 0 \\ 1 & -2 & 1 & \cdots & 0 \\ \vdots & \ddots & \ddots & \ddots & \vdots \\ 0 & \cdots & 1 & -2 & 1 \\ 0 & \cdots & 0 & 1 & -1 \end{bmatrix}. \tag{19}$$

By introducing the auxiliary variable $\boldsymbol{\omega}_m \in \mathbb{R}^{N\times 1}$, the multiple inequality constraints in (18) are transformed into multiple equality constraints, i.e.,

$$\min_{\{\boldsymbol{u}_{i,m}\},\{\boldsymbol{v}_{i,m}\},\{\boldsymbol{f}_i\},\boldsymbol{\omega}_m} \left\{ \sum_{m=1}^{M} \mathcal{I}_{\mathcal{C}_\varepsilon}(\boldsymbol{\omega}_m) + \sum_{i=1}^{Q}\sum_{m=1}^{M} \left(\|\Omega \boldsymbol{u}_{i,m}\|_2^2 + \|\Omega \boldsymbol{v}_{i,m}\|_2^2 \right) \right\}$$
$$s.t. \quad \boldsymbol{\omega}_m = \boldsymbol{x}_m - \sum_{i=1}^{Q} (\boldsymbol{A}_i \boldsymbol{u}_{i,m} + \boldsymbol{B}_i \boldsymbol{v}_{i,m}), \quad m = 1, 2, \ldots, M \tag{20}$$

where $\mathcal{I}_{\mathcal{C}_\varepsilon}(\cdot)$ is an indicator function

$$\mathcal{I}_{\mathcal{C}_\varepsilon}(\boldsymbol{\omega}) \triangleq \begin{cases} 0, & \boldsymbol{\omega} \in \mathcal{C}_\varepsilon \\ +\infty & \boldsymbol{\omega} \notin \mathcal{C}_\varepsilon \end{cases} \tag{21}$$

where $\mathcal{C}_\varepsilon$ is an Euclidean ball with the center of zero and radius of ε, i.e. $\mathcal{C}_{\varepsilon_m} \triangleq \left\{ c \in \mathbb{R}^{N\times 1} : \|c\|_2 \le \varepsilon_m \right\}$. It is notable that, as opposed to many methods, such as MEMD and MVMD, the influence of noise is taken into account by including the auxiliary (or noise) variable $\boldsymbol{\omega}_m \in \mathbb{R}^{N\times 1}$. As a result, the proposed approach will outperform MVMD in noisy environment. The corresponding augmented Lagrangian function of (20) then becomes

$$\begin{aligned} L_\alpha\left(\{\boldsymbol{u}_{i,m}\}, \{\boldsymbol{v}_{i,m}\}, \{\boldsymbol{f}_i\}, \boldsymbol{\omega}_m, \boldsymbol{\lambda}_m\right) &= \sum_{m=1}^{M} \mathcal{I}_{\mathcal{C}_{\varepsilon_m}}(\boldsymbol{\omega}_m) \\ &+ \sum_{i=1}^{Q}\sum_{m=1}^{M} \left(\|\Omega \boldsymbol{u}_{i,m}\|_2^2 + \|\Omega \boldsymbol{v}_{i,m}\|_2^2 \right) \\ &+ \sum_{m=1}^{M} \boldsymbol{\lambda}_m^T \left(\boldsymbol{\omega}_m + \sum_{i=1}^{Q} (\boldsymbol{A}_i \boldsymbol{u}_{i,m} + \boldsymbol{B}_i \boldsymbol{v}_{i,m}) - \boldsymbol{x}_m \right) \\ &+ \sum_{m=1}^{M} \frac{\alpha}{2} \left\| \boldsymbol{\omega}_m + \sum_{i=1}^{Q} (\boldsymbol{A}_i \boldsymbol{u}_{i,m} + \boldsymbol{B}_i \boldsymbol{v}_{i,m}) - \boldsymbol{x}_m \right\|_2^2 \end{aligned} \tag{22}$$

where $\boldsymbol{\lambda}_m \in \mathbb{R}^{N\times 1}$ is the Lagrangian multiplier and α is a quadratic penalty parameter. According to Appendix A, (22) is equivalent to

$$\begin{aligned} L_\alpha\left(\{\boldsymbol{u}_{i,m}\}, \{\boldsymbol{v}_{i,m}\}, \{\boldsymbol{f}_i\}, \boldsymbol{\omega}_m, \boldsymbol{\lambda}_m\right) &= \sum_{m=1}^{M} \mathcal{I}_{\mathcal{C}_{\varepsilon_m}}(\boldsymbol{\omega}_m) \\ &+ \sum_{i=1}^{Q}\sum_{m=1}^{M} \left(\|\Omega \boldsymbol{u}_{i,m}\|_2^2 + \|\Omega \boldsymbol{v}_{i,m}\|_2^2 \right) \\ &+ \sum_{m=1}^{M} \left(\frac{\alpha}{2} \left\| \boldsymbol{\omega}_m + \sum_{i=1}^{Q} (\boldsymbol{A}_i \boldsymbol{u}_{i,m} + \boldsymbol{B}_i \boldsymbol{v}_{i,m}) - \boldsymbol{x}_m + \frac{1}{\alpha}\boldsymbol{\lambda}_m \right\|_2^2 \right. \\ &\left. - \frac{1}{2\alpha} \|\boldsymbol{\lambda}_m\|_2^2 \right). \end{aligned} \tag{23}$$

Then, the solution of the original minimization problem (18) is found as the saddle point of the augmented Lagrangian (23) in a sequence of iterative sub-optimizations termed alternate direction method of multipliers (ADMM) [40]. This optimization problem can be divided into three sub-problems [2], i.e., the update of auxiliary variable ($\boldsymbol{\omega}$), demodulated signals ($\boldsymbol{u}$, $\boldsymbol{v}$), instantaneous frequencies $\boldsymbol{f}$. The adopted method is a variant ADMM rather than the standard version. We will detail how the respective sub-problems can be solved in the following. For notational simplicity, the iteration counters (i.e., superscripts like $\cdot^k$) are omitted, and each is implicitly understood as the most recent available update.

3.3.1. Update w.r.t. auxiliary variable

The update of the auxiliary $\boldsymbol{\omega}_m$ variable can be obtained by solving the following sub-problem

$$\begin{aligned} \boldsymbol{\omega}_m^{k+1} &= \arg\min_{\boldsymbol{\omega}_m} \left\{ L_\alpha\left(\{\boldsymbol{u}_{i,m}\}, \{\boldsymbol{v}_{i,m}\}, \{\boldsymbol{f}_i\}, \boldsymbol{\omega}_m, \boldsymbol{\lambda}_m\right) \right\} \\ &= \arg\min_{\boldsymbol{\omega}_m} \left\{ \mathcal{I}_{\mathcal{C}_{\varepsilon_m}}(\boldsymbol{\omega}_m) + \frac{\alpha}{2} \left\| \boldsymbol{\omega}_m + \sum_{i=1}^{Q} (\boldsymbol{A}_i \boldsymbol{u}_{i,m} + \boldsymbol{B}_i \boldsymbol{v}_{i,m}) \right. \right. \\ &\left. \left. - \boldsymbol{x}_m + \frac{1}{\alpha}\boldsymbol{\lambda}_m \right\|_2^2 \right\}. \end{aligned} \tag{24}$$

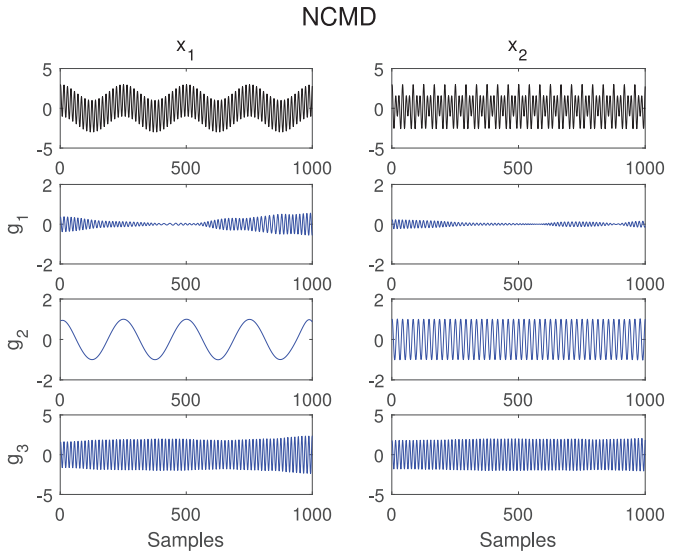

Fig. 3. Decomposition of a bivariate signal consisting of a mixture of tones via univariate NCMD. Note that mode 2 decomposition is misaligned.

The corresponding solution of (24) is given by

$$\boldsymbol{\omega}_m^{k+1} = \mathcal{P}_{\mathcal{C}_{\varepsilon_m}}\left(\boldsymbol{x}_m - \sum_{i=1}^{Q}\left(\boldsymbol{A}_i\boldsymbol{u}_{i,m} + \boldsymbol{B}_i\boldsymbol{v}_{i,m}\right) - \frac{1}{\alpha}\boldsymbol{\lambda}_m\right) \tag{25}$$

where $\mathcal{P}_{\mathcal{C}_{\varepsilon_m}}(\cdot)$ is a proximity operator [41], defined as

$$\mathrm{prox}_{\mathcal{C}_{\varepsilon_m}/\alpha}(\boldsymbol{z}) = \mathcal{P}_{\mathcal{C}_{\varepsilon_m}}(\boldsymbol{z}) \triangleq \begin{cases} \frac{\varepsilon_m}{\|\boldsymbol{z}\|_2}\cdot\boldsymbol{z}, & \|\boldsymbol{z}\|_2 > \varepsilon_m \\ \boldsymbol{z}, & \|\boldsymbol{z}\|_2 \le \varepsilon_m \end{cases}. \tag{26}$$

3.3.2. Update w.r.t. demodulated signals

Following, the demodulated quadrature signals $\boldsymbol{u}_{i,m}$ and $\boldsymbol{v}_{i,m}$ can be updated as

$$\begin{aligned}\boldsymbol{u}_{i,m}^{k+1} &= \arg\min_{\boldsymbol{u}_{i,m}}\left\{L_\alpha\left(\{\boldsymbol{u}_{j,m}\},\{\boldsymbol{v}_{j,m}\},\{\boldsymbol{f}_j\},\boldsymbol{\omega}_m,\boldsymbol{\lambda}_m\right)\right\} \\ &= \arg\min_{\boldsymbol{u}_{i,m}}\left\{\|\Omega\boldsymbol{u}_{i,m}\|_2^2 + \frac{\alpha}{2}\left\|\boldsymbol{\omega}_m + \sum_{j=1}^{Q}\left(\boldsymbol{A}_j\boldsymbol{u}_{j,m} + \boldsymbol{B}_j\boldsymbol{v}_{j,m}\right)\right.\right. \\ &\qquad \left.\left. - \boldsymbol{x}_m + \frac{1}{\alpha}\boldsymbol{\lambda}_m\right\|_2^2\right\}. \end{aligned} \tag{27}$$

$$\begin{aligned}\boldsymbol{v}_{i,m}^{k+1} &= \arg\min_{\boldsymbol{v}_{i,m}}\left\{L_\alpha\left(\{\boldsymbol{u}_{j,m}\},\{\boldsymbol{v}_{j,m}\},\{\boldsymbol{f}_j\},\boldsymbol{\omega}_m,\boldsymbol{\lambda}_m\right)\right\} \\ &= \arg\min_{\boldsymbol{v}_{i,m}}\left\{\|\Omega\boldsymbol{v}_{i,m}\|_2^2 + \frac{\alpha}{2}\left\|\boldsymbol{\omega}_m + \sum_{j=1}^{Q}\left(\boldsymbol{A}_j\boldsymbol{u}_{j,m} + \boldsymbol{B}_j\boldsymbol{v}_{j,m}\right)\right.\right. \\ &\qquad \left.\left. - \boldsymbol{x}_m + \frac{1}{\alpha}\boldsymbol{\lambda}_m\right\|_2^2\right\}. \end{aligned} \tag{28}$$

(27) and (28) can be easily solved by setting their gradients to zero, yielding

$$\boldsymbol{u}_{i,m}^{k+1} = \underbrace{\left(\frac{2\Omega^T\Omega}{\alpha} + \boldsymbol{A}_i^T\boldsymbol{A}_i\right)^{-1}}_{\boldsymbol{H}_{c_{i,m}}}\boldsymbol{A}_i^T\underbrace{\left(\boldsymbol{x}_m - \sum_{j\neq i}^{Q}\boldsymbol{A}_j\boldsymbol{u}_{j,m} - \sum_{j=1}^{Q}\boldsymbol{B}_j\boldsymbol{v}_{j,m} - \boldsymbol{\omega}_m - \frac{1}{\alpha}\boldsymbol{\lambda}_m\right)}_{\boldsymbol{r}_{c_{i,m}}} \tag{29}$$

$$\boldsymbol{v}_{i,m}^{k+1} = \underbrace{\left(\frac{2\Omega^T\Omega}{\alpha} + \boldsymbol{B}_i^T\boldsymbol{B}_i\right)^{-1}}_{\boldsymbol{H}_{s_{i,m}}}\boldsymbol{B}_i^T\underbrace{\left(\boldsymbol{x}_m - \sum_{j=1}^{Q}\boldsymbol{A}_j\boldsymbol{u}_{j,m} - \sum_{j\neq i}^{Q}\boldsymbol{B}_j\boldsymbol{v}_{j,m} - \boldsymbol{\omega}_m - \frac{1}{\alpha}\boldsymbol{\lambda}_m\right)}_{\boldsymbol{r}_{s_{i,m}}} \tag{30}$$

where $\boldsymbol{H}_{c_{i,m}}$ and $\boldsymbol{H}_{s_{i,m}}$ act as two time-frequency filters, which are similar to those in NCMD.

3.3.3. Update w.r.t. instantaneous frequency

Now, we turn our attention to the optimization problem corresponding to instantaneous frequency update. It is observed that the instantaneous frequencies are not explicitly represented in the corresponding augmented Lagrangian function (22); while other variables are explicitly represented. Therefore, we cannot get the update formula about instantaneous frequencies as the way we treat other variables. It is necessary to seek another way to tackle this problem. Notice that the two demodulated signals $\boldsymbol{u}(t)$ (14) and

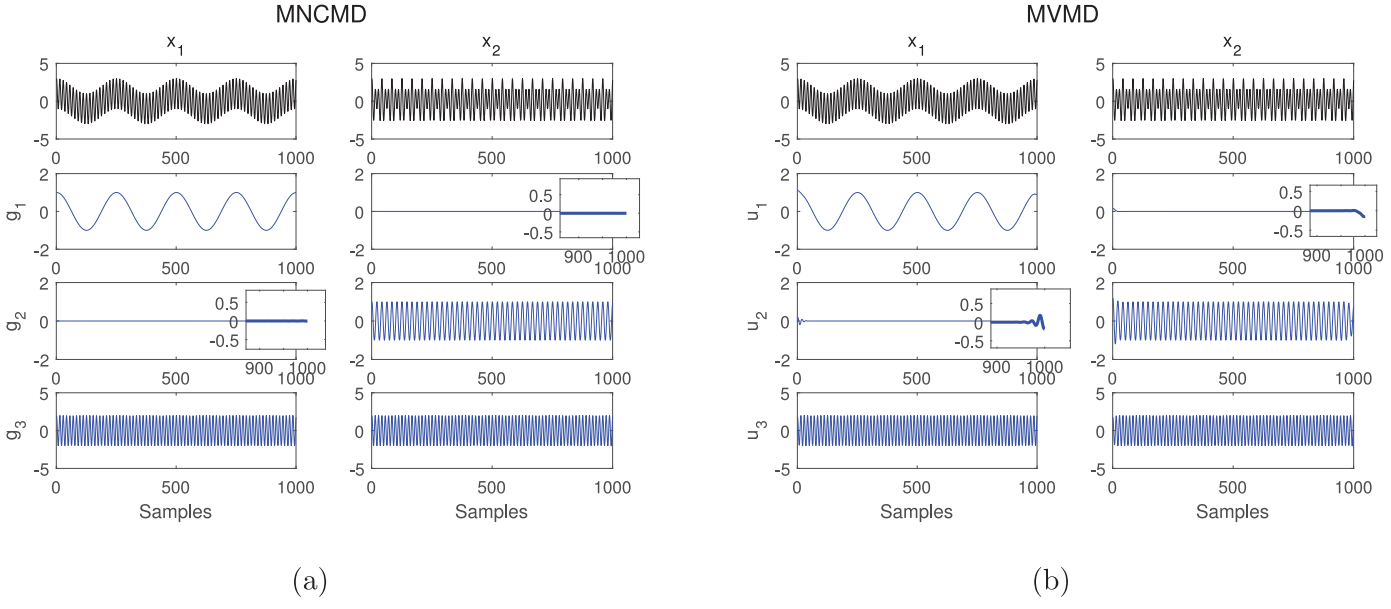

Fig. 4. Decomposition of a bivariate signal consisting of a mixture of tones via (a) MNCMD and (b) MVMD. Both methods show mode-alignment property but MVMD suffers from end-effect.

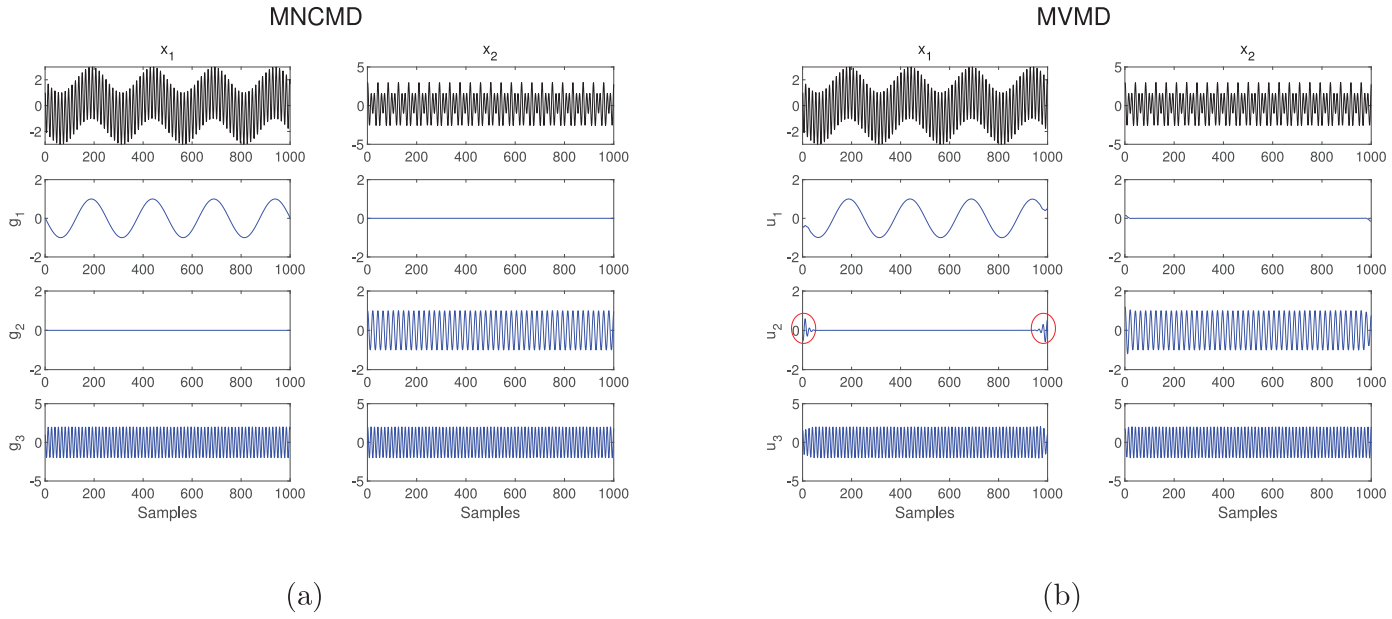

Fig. 5. Decomposition of a bivariate signal with phase shifts via (a) MNCMD and (b) MVMD. Both methods show mode-alignment property but MVMD is subjected to end-effect issue (marked with ellipses).

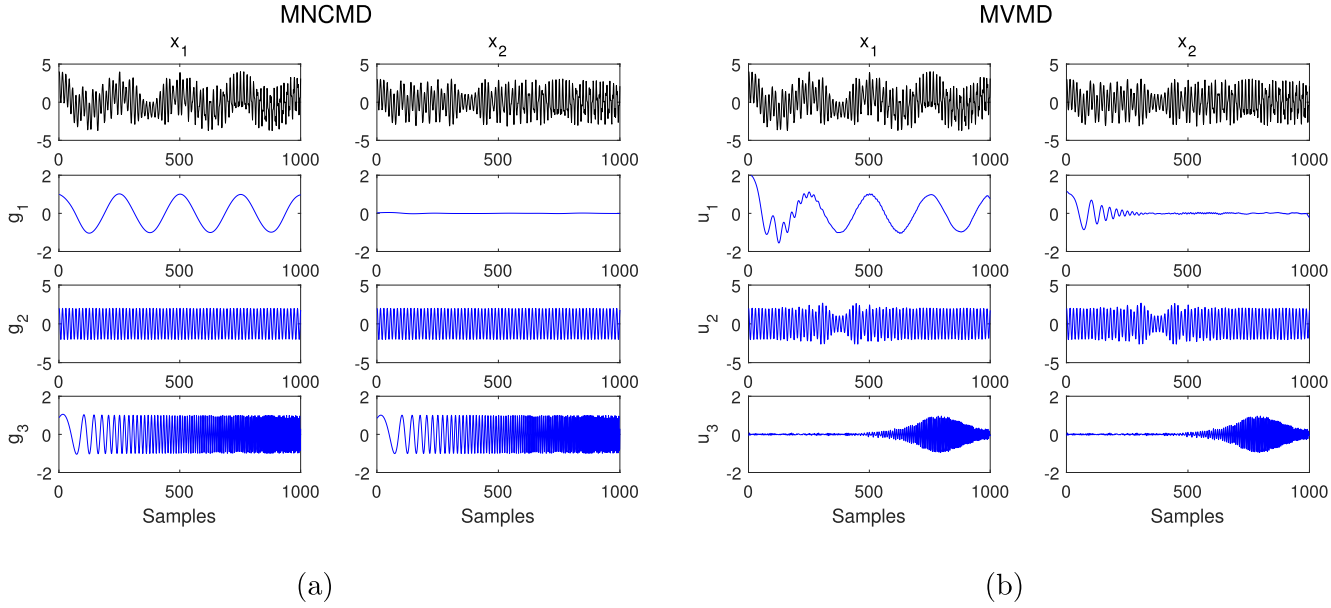

Fig. 6. Decomposition of a bivariate signal with frequency varying linearly via (a) MNCMD and (b) MVMD. Note that MNCMD shows satisfied mode-alignment property and extracts all modes correctly while MVMD fails to process such signals.

$\boldsymbol{v}(t)$ (15) could provide the increment information for the IFs [2]. Having updated $\boldsymbol{u}_{i,m}$ and $\boldsymbol{v}_{i,m}$, the increment information for the IFs can be obtained by arctangent demodulation approach [42], as shown in (31).

$$\begin{aligned}\Delta\tilde{f}_{i,m}^{k+1}(t) &= -\frac{1}{2\pi}\frac{d}{dt}\left(\arctan\left(\frac{v_{i,m}^{k+1}(t)}{u_{i,m}^{k+1}(t)}\right)\right)\\ &= \frac{v_{i,m}^{k+1}(t)\cdot\left(u_{i,m}^{k+1}(t)\right)' - u_{i,m}^{k+1}(t)\cdot\left(v_{i,m}^{k+1}(t)\right)'}{2\pi\left(\left(u_{i,m}^{k+1}(t)\right)^2+\left(v_{i,m}^{k+1}(t)\right)^2\right)}.\end{aligned} \tag{31}$$

Note that in this step we only obtain the increment of IF rather than the IF itself. Then the IF can be calculated as

$$\boldsymbol{f}_{i,m}^{k+1} = \boldsymbol{f}_{i,m}^{k} + \gamma\cdot\Delta\tilde{\boldsymbol{f}}_{i,m}^{k+1}. \tag{32}$$

where γ is a proportionality factor.

However, due to the limitations of arctangent demodulation and noise, the current increment of instantaneous frequency $\Delta\tilde{\boldsymbol{f}}_{i,m}^{k+1}$ is not smooth enough, which would result in the unsmooth instantaneous frequency. This is not consistent with the requirement in nonlinear chirp mode that the instantaneous frequency should be smooth enough. In order to remedy this issue, the increment of instantaneous frequency $\Delta\tilde{\boldsymbol{f}}_{i,m}^{k+1}$ is filtered by a low-pass filter. The corresponding filter can be obtained by solving the problem

$$\min_{\Delta\boldsymbol{f}_{i,m}^{k+1}}\left\{\left\|\Omega\Delta\boldsymbol{f}_{i,m}^{k+1}\right\|_2^2+\frac{\mu}{2}\left\|\Delta\boldsymbol{f}_{i,m}^{k+1}-\Delta\tilde{\boldsymbol{f}}_{i,m}^{k+1}\right\|_2^2\right\} \tag{33}$$

where μ is a penalty parameter; $\Delta\tilde{\boldsymbol{f}}_{i,m}^{k+1} = \left[\Delta\tilde{f}_{i,m}^{k+1}(t_0), \ldots, \Delta\tilde{f}_{i,m}^{k+1}(t_{N-1})\right]^T$ represents the results of (31) and $\Delta\boldsymbol{f}_{i,m}^{k+1}$ is the desired one, given by

$$\Delta\boldsymbol{f}_{i,m}^{k+1} = \left(\frac{2}{\mu}\Omega^T\Omega + \boldsymbol{I}\right)^{-1}\Delta\tilde{\boldsymbol{f}}_{i,m}^{k+1} \tag{34}$$

where $\boldsymbol{I}$ stands for an identity matrix. In fact, (33) is formulated on the assumption that the increment of IF in each iteration is still a band-limited function [2]. Based on the filtered increment $\Delta\boldsymbol{f}_{i,m}^{k+1}$, the update formula of instantaneous frequency is modified from (32) to (35)

$$\boldsymbol{f}_{i,m}^{k+1} = \boldsymbol{f}_{i,m}^{k} + \gamma\cdot\Delta\boldsymbol{f}_{i,m}^{k+1} \tag{35}$$

where $\gamma = 0.5$ is a proportionality factor adopted to stabilize the algorithm [2].

To summarize, the update of instantaneous frequency is

$$\begin{aligned}\boldsymbol{f}_{i,m}^{k+1} &= \boldsymbol{f}_{i,m}^{k} + \gamma\cdot\Delta\boldsymbol{f}_{i,m}^{k+1}\\ &= \boldsymbol{f}_{i,m}^{k} + \gamma\cdot\underbrace{\left(\frac{2}{\mu}\Omega^T\Omega + \boldsymbol{I}\right)^{-1}}_{filter}\Delta\tilde{\boldsymbol{f}}_{i,m}^{k+1}\\ &= \boldsymbol{f}_{i,m}^{k} + \gamma\cdot\underbrace{\left(\frac{2}{\mu}\Omega^T\Omega + \boldsymbol{I}\right)^{-1}}_{filter}\\ &\quad\times\left(-\frac{1}{2\pi}\frac{d}{dt}\left(\arctan\left(\frac{v_{i,m}^{k+1}(t)}{u_{i,m}^{k+1}(t)}\right)\right)\right)\end{aligned} \tag{36}$$

where the filter acts low-pass property to ensure smoothness.

Note that, (35) is the instantaneous frequency of mode i and channel m. However, the multivariate signal decomposition method requires all channels present a joint or common frequency, which is a problem that must be solved for MNCMD. MVMD solves this problem in frequency domain [1]. More specifically, it updates the center frequency by taking the contributions from power spectrum of all channels into account, namely, the center frequency of each channel is weighted and averaged according to its signal spectrum. For the proposed MNCMD, updating formulas in the form of frequency domain is not available. Inspired by Parseval theorem, the above operations in the frequency domain can be performed in the time domain equivalently. In this work, the common frequency information is obtained by the *power-weighted* average of the instantaneous frequency of each channel. The weighting factor is the instantaneous energy of each channel, which is equivalent to the energy of spectrum in frequency domain. As a result, the instantaneous frequency is given below

$$\boldsymbol{f}_i^{k+1}(t_n) = \frac{\sum_{m=1}^{M}\boldsymbol{f}_{i,m}^{k+1}(t_n)\left|\boldsymbol{a}_{i,m}^{k+1}(t_n)\right|^2}{\sum_{m=1}^{M}\left|\boldsymbol{a}_{i,m}^{k+1}(t_n)\right|^2} \tag{37}$$

where $\boldsymbol{a}_{i,m}^{k+1} = \sqrt{\left(\boldsymbol{u}_{i,m}^{k+1}\right)^2 + \left(\boldsymbol{v}_{i,m}^{k+1}\right)^2}$ is the instantaneous amplitude. More discussion on (37) is provided in Appendix B.

The last step of MNCMD is to update the Lagrangian multiplier as

$$\boldsymbol{\lambda}_m^{k+1} = \boldsymbol{\lambda}_m^{k} + \alpha\left(\boldsymbol{\omega}_m + \sum_{i=1}^{Q}\boldsymbol{g}_{i,m}^{k+1} - \boldsymbol{x}_m\right). \tag{38}$$

The above steps are summarized in Algorithm 1. It is worth noting that the proposed multivariate NCMD does not introduce more user-defined parameters than univariate NCMD. Penalty parameters (i.e. α and μ) play the same role for MNCMD and NCMD. Therefore, one could use the same parameters in MNCMD as that adopted in NCMD. The properties and advantages of univariate NCMD have been explored in detail in [2].

Algorithm 1 Multivariate nonlinear chirp mode decomposition.

Initialize: $\boldsymbol{x_m}$, α, μ, $\boldsymbol{f}_i$, $\boldsymbol{A}_i = diag\left[\cos\left(2\pi\int f_i^1(t)dt\right)\right]$, $\boldsymbol{B}_i = diag\left[\sin\left(2\pi\int f_i^1(t)dt\right)\right]$, $\boldsymbol{u}_{i,m}^1 = \left(\frac{2}{\alpha}\Omega^T\Omega + \left(\boldsymbol{A}_i^1\right)^T\boldsymbol{A}_i^1\right)^{-1}\left(\boldsymbol{A}_i^1\right)^T\boldsymbol{x}_m$, $\boldsymbol{v}_{i,m}^1 = \left(\frac{2}{\alpha}\Omega^T\Omega + \left(\boldsymbol{B}_i^1\right)^T\boldsymbol{B}_i^1\right)^{-1}\left(\boldsymbol{B}_i^1\right)^T\boldsymbol{x}_m$, $\boldsymbol{\lambda}_m^1 = \boldsymbol{0}$, for $i = 1, \ldots, Q$, $m = 1, \ldots, M$; $k = 0$

while $\sum_{i=1}^{Q}\sum_{m=1}^{M}\frac{\left\|\boldsymbol{g}_{i,m}^{k+1} - \boldsymbol{g}_{i,m}^{k}\right\|_2^2}{\left\|\boldsymbol{g}_{i,m}^{k}\right\|_2^2} > \delta$ **do**

  $k = k + 1$

  for $m = 1 : M$ **do**

    $\boldsymbol{\omega}_m^{k+1} = \mathcal{P}_{\mathcal{C}_{\varepsilon_m}}\left(\boldsymbol{x}_m - \sum_{i=1}^{Q}\left(\boldsymbol{A}_i\boldsymbol{u}_{i,m} + \boldsymbol{B}_i\boldsymbol{v}_{i,m}\right) - \frac{1}{\alpha}\boldsymbol{\lambda}_m\right)$

  end for

  for $i = 1 : Q$ **do**

    $\boldsymbol{A}_i^{k+1} = diag\left[\cos\left(2\pi\int f_i^{k+1}(t)dt\right)\right]$

    $\boldsymbol{B}_i^{k+1} = diag\left[\sin\left(2\pi\int f_i^{k+1}(t)dt\right)\right]$

    for $m = 1 : M$ **do**

      $\boldsymbol{u}_{i,m}^{k+1} = \arg\min_{\boldsymbol{u}_{i,m}}\left\{L_\alpha\left(\left\{\boldsymbol{u}_{j,m}\right\}, \left\{\boldsymbol{v}_{j,m}\right\}, \left\{\boldsymbol{f}_j\right\}, \boldsymbol{\omega}_m, \boldsymbol{\lambda}_m\right)\right\}$

      $\boldsymbol{v}_{i,m}^{k+1} = \arg\min_{\boldsymbol{v}_{i,m}}\left\{L_\alpha\left(\left\{\boldsymbol{u}_{j,m}\right\}, \left\{\boldsymbol{v}_{j,m}\right\}, \left\{\boldsymbol{f}_j\right\}, \boldsymbol{\omega}_m, \boldsymbol{\lambda}_m\right)\right\}$

      $\boldsymbol{a}_{i,m}^{k+1} = \sqrt{\left(\boldsymbol{u}_{i,m}^{k+1}\right)^2 + \left(\boldsymbol{v}_{i,m}^{k+1}\right)^2}$

      $\Delta\tilde{f}_{i,m}^{k+1}(t) = \frac{v_{i,m}^{k+1}(t)\cdot\left(u_{i,m}^{k+1}(t)\right)' - u_{i,m}^{k+1}(t)\cdot\left(v_{i,m}^{k+1}(t)\right)'}{2\pi\left(\left(u_{i,m}^{k+1}(t)\right)^2 + \left(v_{i,m}^{k+1}(t)\right)^2\right)}$

      $\boldsymbol{f}_{i,m}^{k+1} = \boldsymbol{f}_{i,m}^{k} + \gamma\cdot\left(\frac{2}{\mu}\Omega^T\Omega + \boldsymbol{I}\right)^{-1}\Delta\tilde{\boldsymbol{f}}_{i,m}^{k+1}$

    end for

    $\boldsymbol{f}_i^{k+1}(t_n) = \frac{\sum_{m=1}^{M}\boldsymbol{f}_{i,m}^{k+1}(t_n)\left|\boldsymbol{a}_{i,m}^{k+1}(t_n)\right|^2}{\sum_{m=1}^{M}\left|\boldsymbol{a}_{i,m}^{k+1}(t_n)\right|^2}$

    for $m = 1 : M$ **do**

      $\mathbf{g}_{i,m}^{k+1} = \mathbf{A}_i\mathbf{u}_{i,m}^{k+1} + \mathbf{B}_i\mathbf{v}_{i,m}^{k+1}$

    end for

  end for

  for $m = 1 : M$ **do**

    $\lambda_m^{k+1} = \lambda_m^{k} + \alpha\left(\omega_m + \sum_{i=1}^{Q}\boldsymbol{g}_{i,m}^{k+1} - \mathbf{x}_m\right)$

  end for

end while

4. Properties and comparisons

In order to demonstrate the effectiveness and advantages of the proposed MNCMD, this section reports simulations and experiments on a wide range of multivariate data. Specifically, we highlight the mode-alignment property, filter bank structure, quasi-orthogonality, influence of channel number, noise robustness, and convergence. Because MVMD has shown better performance than other methods [1], and it is the latest and promising multivariate signal decomposition algorithm, MNCMD is mainly compared with MVMD.

4.1. Mode-alignment

In this section, we focus on the ability of MNCMD to align common frequency scales across multiple signal channels, which is termed as mode-alignment. Mode-alignment is an critical requirement in many engineering and scientific applications including image fusion [43], denoising [44], disease diagnosis [29], to name a few. Detailed discussion on the importance of mode-alignment in signal processing applications are provided in [45].

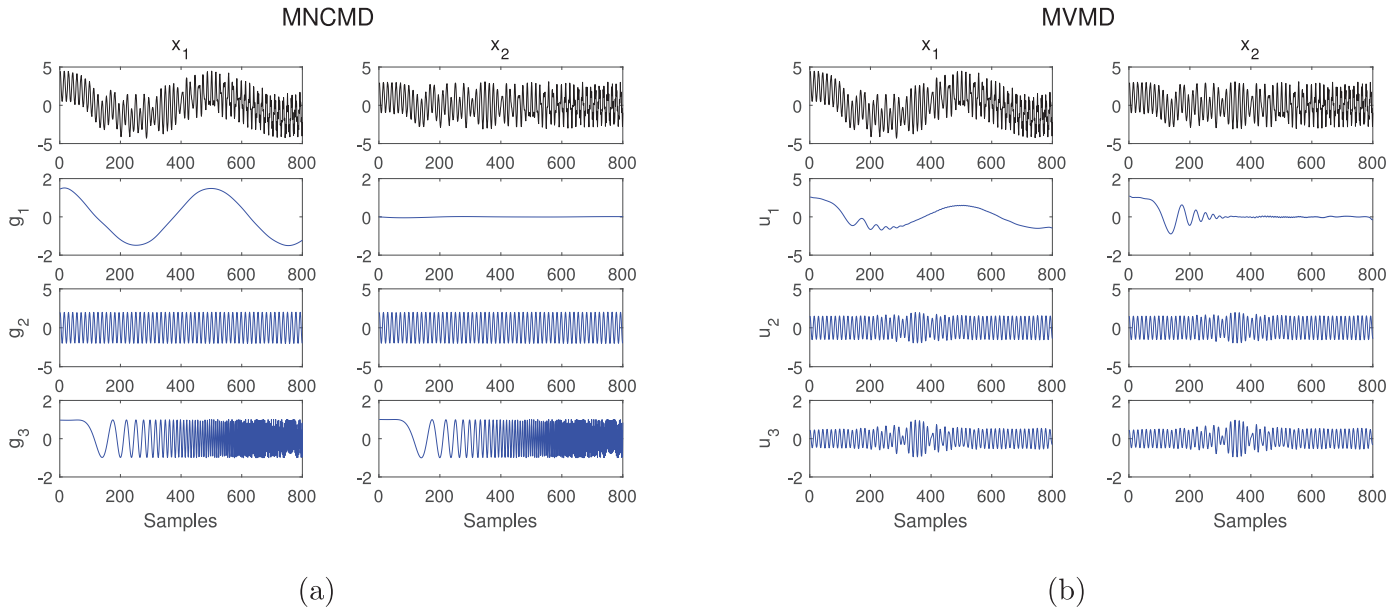

Fig. 7. Decomposition of a bivariate signal with frequency varying nonlinearly via (a) MNCMD and (b) MVMD. Note that MNCMD shows satisfied mode-alignment property and extracts all modes correctly while MVMD fails to process such signals.

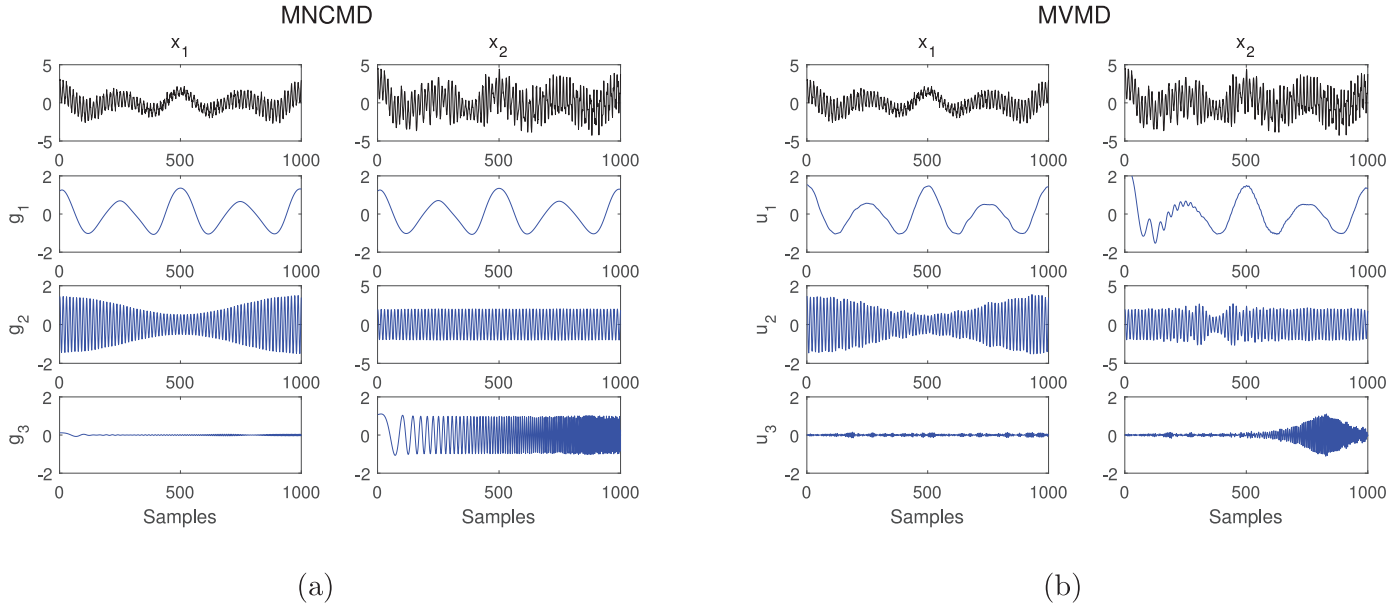

Fig. 8. Decomposition of a bivariate signal with both amplitude and frequency varying via (a) MNCMD and (b) MVMD. Note that MNCMD shows satisfied mode-alignment property while MVMD fails to process such signals.

4.1.1. Case 1: Time-invariant signal

Herein, we consider a signal (39) consisting of two channels. The individual components are a mixture of 36-Hz sinusoid that was common to both data channels; a 2-Hz tone in $x_1(t)$ (channel 1), and a 24-Hz tone in the $x_2(t)$ (channel-2).

$$\begin{cases} x_1(t) = \cos(2\pi 2t) + 2\cos(2\pi 36t) \\ x_2(t) = \cos(2\pi 24t) + 2\cos(2\pi 36t) \end{cases} \tag{39}$$

In Fig. 3, signal (39) is decomposed by applying univariate NCMD to each channel separately. Note that the frequency content across channels in mode g_2 is not aligned, i.e., 2-Hz in channel-1 and 24-Hz in channel-2. In addition, there are a lot of energies leaking to mode g_1, whose curves should be lines ideally. The decomposition results of MNCMD and MVMD are displayed in Fig. 4 (a) and (b), respectively. It is observed that all modes are aligned in terms of their frequency contents: the 36-Hz tone presented in all data channels is localized in the third mode. The 2-Hz component is located in the first mode of channel-1 while the 24-Hz signal is localized in the second mode of channel-2. Therefore, like MVMD, the proposed MNCMD also has attractive mode-alignment property. Note that, comparing the endpoints of mode $g_{2,1}$, $g_{1,2}$, $u_{2,1}$, and $u_{1,2}$ in Fig. 4(a) and (b), these modes ($g_{2,1}$ and $g_{1,2}$) obtained by MNCMD are almost a straight line while there are fluctuations in $u_{2,1}$ and $u_{1,2}$. This means MVMD suffers from end-effect, which is a common issue in signal decomposition. Accordingly, both MNCMD and MVMD can align the similar frequency content in a single mode across all signal channels, and MNCMD is less prone to end-effect.

In order to demonstrate the presented MNCMD is able to process signals with phase shifts. (40) is generated by embedding the

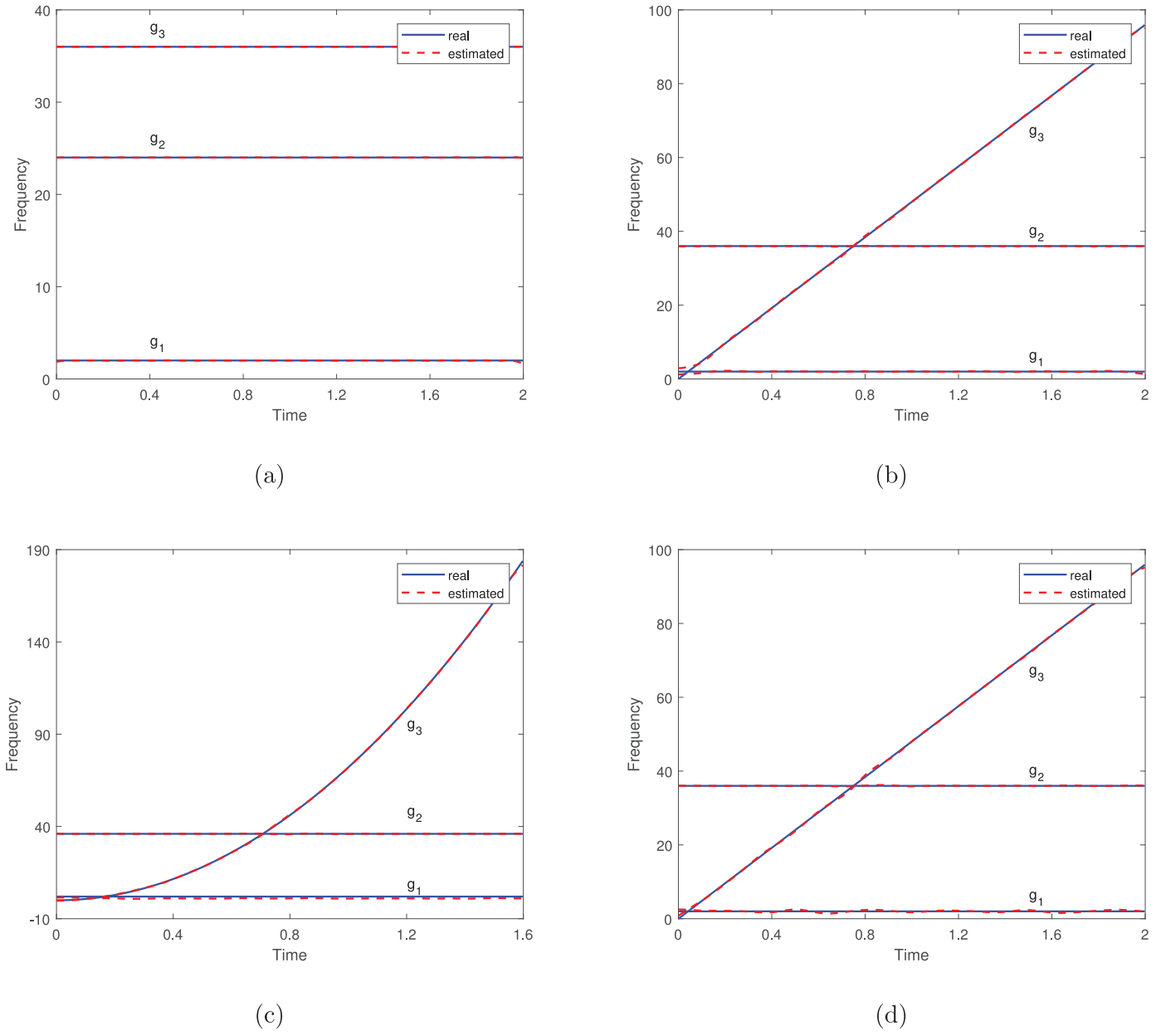

Fig. 9. The estimated IFs by MNCMD for multivariate signals in (a) case 1, (b) case 2, (c) case 3, and (d) case 4. (Blue: true; Red: estimated. For interpretation of the references to colors in this figure, the reader is referred to the web version of this article.) The proposed MNCMD could accurately capture IFs in various cases.

phase shifts across various channels in (39).

$$\begin{cases} x_1(t) = \cos(2\pi 2t + \pi/2) + 2\cos(2\pi 36t + \pi/3) \\ x_2(t) = \cos(2\pi 24t) + 2\cos(2\pi 36t) \end{cases} \tag{40}$$

The decomposition results of MNCMD and MVMD are displayed in Fig. 5 (a) and (b), respectively. It is observed that MVMD suffers from apparent end-effect issue (marked with ellipses); while the MNCMD manifests satisfactory performance. Therefore, the presented MNCMD is not affected by phase shifts.

4.1.2. Case 2: Signal with frequency varying linearly

In this case, MNCMD is applied to a multivariate signal with time-varying frequency, given by

$$\begin{cases} x_1(t) = \cos(2\pi 2t) + 2\cos(2\pi 36t) + \cos\left(2\pi 24t^2\right) + \eta \\ x_2(t) = 2\cos(2\pi 36t) + \cos\left(2\pi 24t^2\right) + \eta \end{cases}, \eta \in \mathcal{N}(0, 0.1). \tag{41}$$

Both channels of signal (41) contain a common time-varying instantaneous frequency $48t$. Fig. 6 (a) and (b) exhibit the decomposition outputs of MNCMD and MVMD, respectively. It can be observed that all modes, including frequency-varying modes, are aligned among all channels in MNCMD; while MVMD not only fails to process the frequency-varying components, but also cannot extract the tones with constant frequency. Therefore, MNCMD outperforms MVMD in decomposing frequency-varying signals and it still can keep the modes aligned in such case.

4.1.3. Case 3: Signal with frequency varying nonlinearly

Then, a more complex multivariate signal (42) with frequency nonlinearly varying is studied.

$$\begin{cases} x_1(t) = 1.5\cos(2\pi 2t) + 2\cos(2\pi 36t) + \cos\left(2\pi 24t^3\right)\eta \\ x_2(t) = 2\cos(2\pi 36t) + \cos\left(2\pi 24t^3\right) + \eta \end{cases}, \eta \in \mathcal{N}(0, 0.1). \tag{42}$$

It is apparent that there is a nonlinear varying frequency $\left(2\pi 24t^3\right)'/2\pi = 72t^2$ in (42). The corresponding decomposition

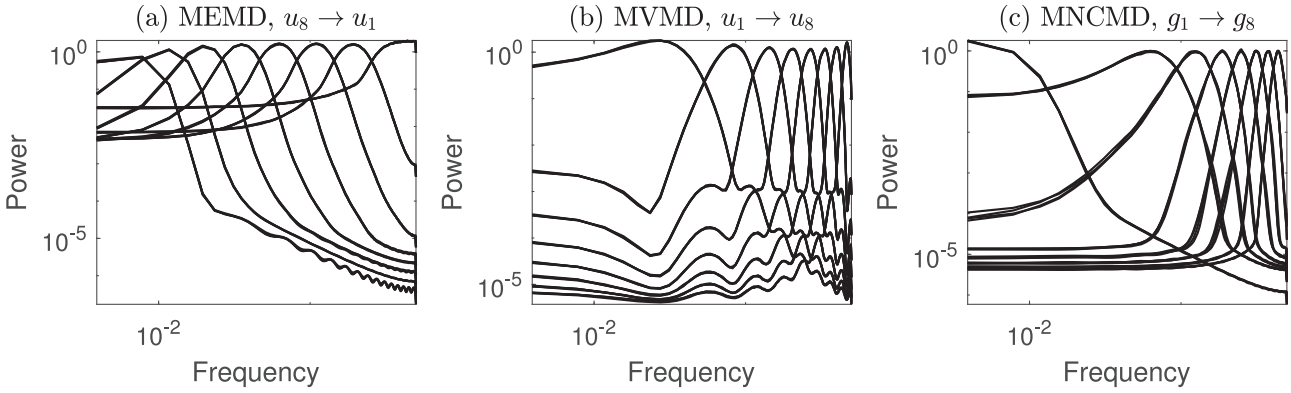

Fig. 10. Filter bank structure of (a) MEMD, (b) MVMD, (c) MNCMD for four-channel wGn. Both MVMD and MNCMD follow a different filter bank structure as compared to the quasi-dyadic filter bank of MEMD. The mode-alignment across channels is clear in all three cases.

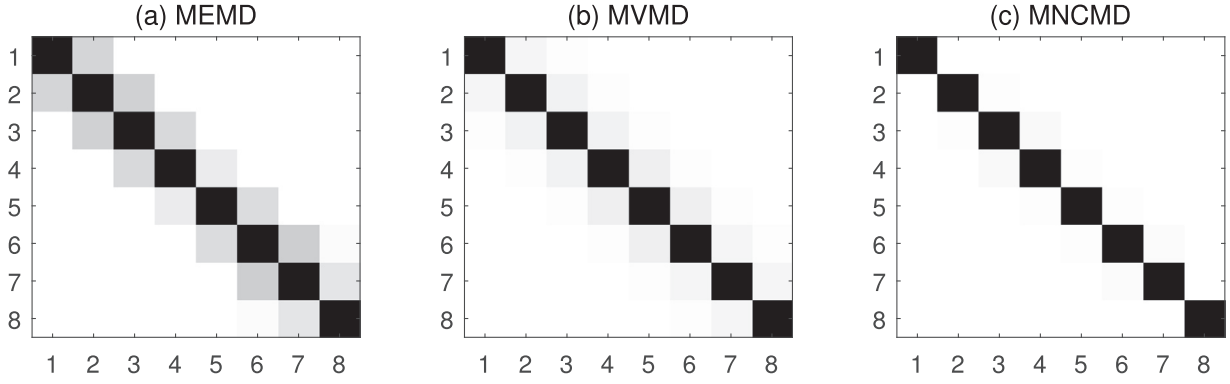

Fig. 11. Illustration of quasi-orthogonality of decomposed modes obtained from (a) MEMD, (b) MVMD, and (c) MNCMD for a four-channel wGn. The correlation coefficient matrices are transformed into a set of gray-scale images, in which black and white represent 1 and 0 respectively. Note that, in MNCMD, the gray parts are minimum and the color is the lightest, which indicates the best quasi-orthogonality.

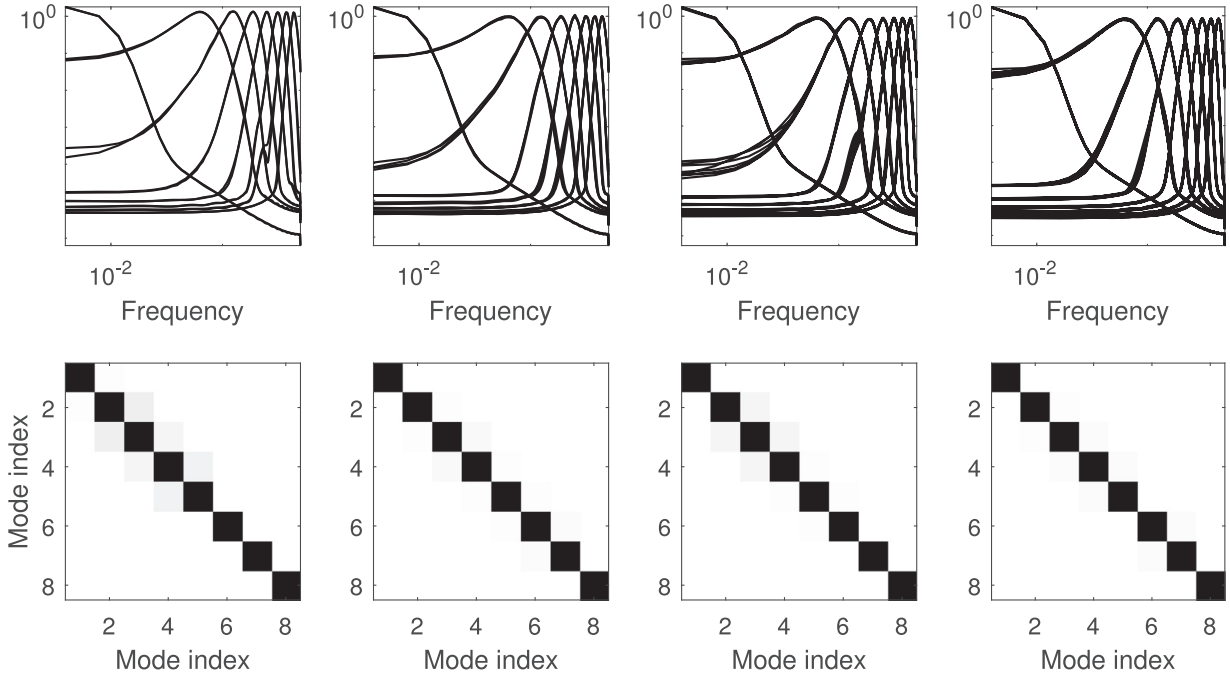

Fig. 12. MNCMD decomposition of wGn for increasing signal channels. (First row) Illustration of the mode-alignment property, filter bank structure of MNCMD for increasing signal channels, i.e., $M = 2, 4, 8,$ and 16 from left to right respectively. (Second row) Illustration of quasi-orthogonality of MNCMD for increasing signal channels i.e., $M = 2, 4, 8,$ and 16 from left to right respectively. Note that different channel number does not affect the performance of MNCMD in terms of mode-alignment, filter bank property and quasi-orthogonality.

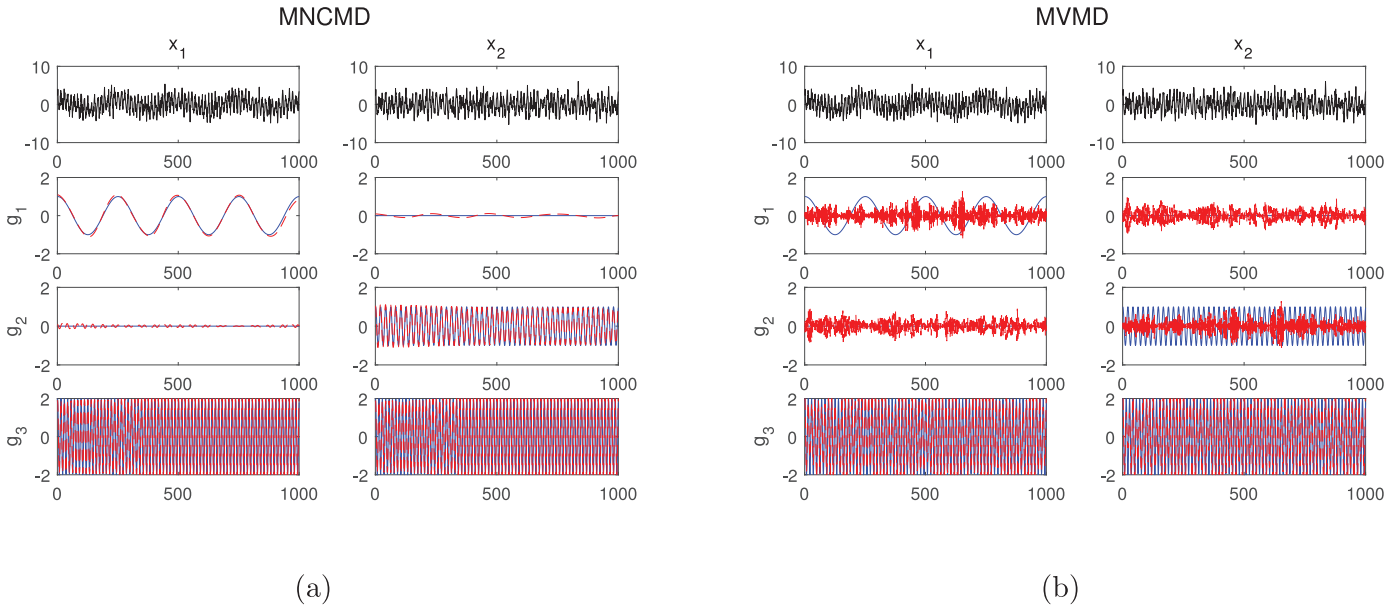

Fig. 13. Decomposition of a bivariate signal consisting of a mixture of tones and noise in both channels via (a) MNCMD and (b) MVMD. The noise variance is 1. (Red: real mode; Blue: estimated mode. For interpretation of the references to colors in this figure, the reader is referred to the web version of this article.) Note that the modes with similar frequency are clearly aligned and correctly extracted in MNCMD. However, the performance of MVMD is heavily degraded by noise. More comparisons are provided in the attached animation.

Table 1
Computation time (in seconds) of the presented method.

Case	1	2	3	4
Time	0.5064	2.6167	3.6437	5.5567

modes of MNCMD and MVMD are shown in Fig. 7 (a) and (b), respectively. From these figures, it can be seen that the multivariate nonlinear chirp modes $g_{3,1}$ and $g_{3,2}$ are extracted correctly and well aligned in terms of their frequency components. On the contrary, MVMD does not correctly decompose the corresponding modes. And the MVMD's mode-alignment phenomenon in Fig. 7(a) is meaningless. This further illustrates MNCMD surpasses MVMD in decomposing time-varying multivariate signals.

4.1.4. Case 4: Signal with amplitude and frequency varying

The last example (43) is a multivariate signal with both amplitude and frequency varying. Fig. 8 (a) and (b) depict the corresponding decomposition results of MNCMD and MVMD, respectively. Like case 2 and 3, MNCMD is able to align all kinds of modes with common frequency and accurately extract the actual modes. By contrast, the performance of MVMD is much worse, which validates that it is not suitable for processing time-varying signals. Consequently, it can be concluded that MNCMD is superior to MVMD in decomposing time-varying multivariate signals.

$$\begin{cases} x_1(t) = (1+0.5\cos(2\pi t))\cos(2\pi\cos(2\pi 2t)) + (1+0.5\cos(\pi t))\cos(2\pi 36t) + \eta \\ x_2(t) = (1+0.5\cos(2\pi t))\cos(2\pi\cos(2\pi 2t)) + 2\cos(2\pi 36t) + \cos\left(2\pi 24t^2\right) + \eta \end{cases}, \quad \eta \in \mathcal{N}(0, 0.2) \tag{43}$$

Fig. 9 shows the estimated instantaneous frequencies of these four cases obtained by MNCMD. It is observed that the estimated IFs are in good agreement with the real frequencies in different cases. Note that MVMD only could provide a center frequency value without time information. Therefore, the proposed MNCMD shows great potential in multivariate time-frequency analysis.

The computation time of the presented method in various cases is reported in Table 1. These data are obtained from a personal computer equipped with an Intel Core i5 Processor, running MATLAB version R2018a, on a 64-bit Windows operating system. It is observed that all cases are processed in a few seconds. Therefore, the calculation efficiency of MNCMD is satisfactory.

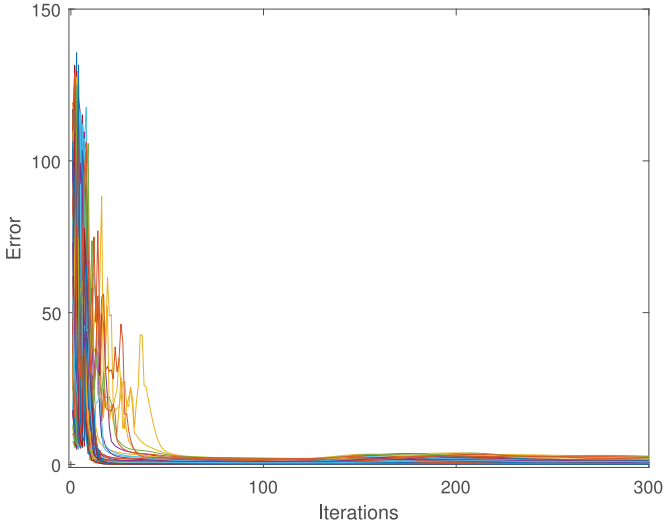

Fig. 14. Convergence curves with 100 random initial instantaneous frequencies.

In summary, the above four examples demonstrate the proposed MNCMD have attractive mode-alignment property and can extract modes correctly, especially for time-varying multivariate signals. On the contrary, MVMD suffers from difficulties when processing data with time-varying characteristics.

4.2. Filter bank structure

A filter bank is an array of band-pass filters that separates the input signal into multiple components, each one carrying a

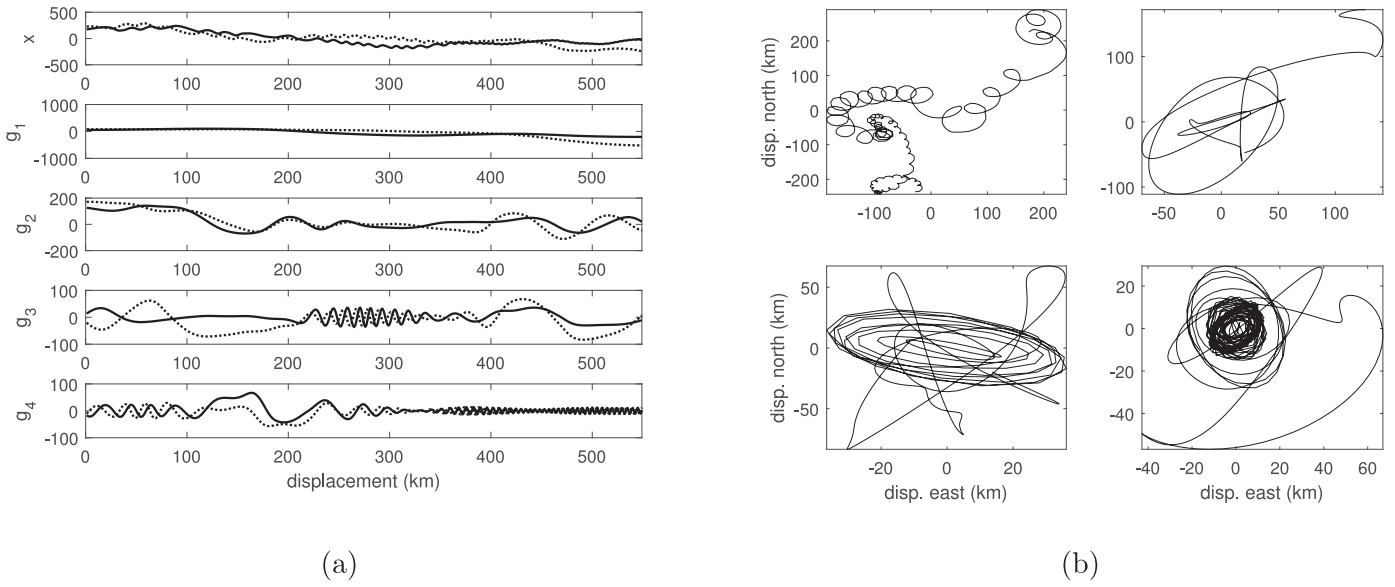

Fig. 15. (a): Time plots of bivariate oscillations and the corresponding modes obtained from MNCMD. (b): 2-D plots of bivariate oscillations (top left) and the corresponding mode 2 (top right), 3 (lower left), and 4 (lower right) obtained from MNCMD.

single frequency sub-band of the original signal [1]. Investigating filter bank structures is useful to understand how a full spectrum process is split into its modes. According to [46], MEMD exhibits quasi-dyadic filter bank structure for wGn (white Gaussian noise), which is similar to the wavelet filter bank. MVMD also shows filter bank structure for wGn, while it is different from the quasi-dyadic property observed within EMD/MEMD-based methods [1].

In this section, MNCMD utilizes the numerical Monte Carlo experiments based on wGn to reveal its filter bank structure. Like the related experiments on MVMD and MEMD, we applied MNCMD on 500 realizations of a four-channel wGn data of length $L = 1000$. The corresponding power spectra of MEMD, MVMD, and MNCMD are plotted in Fig. 10. Comparing these three sets of graphs, it can be seen that both MNCMD and MVMD follow a different filter band structure as compared to the quasi-dyadic filterbank property of MEMD. The bandwidths of MEMD's modes are almost similar in the log-frequency domain. While those of the other two decomposition methods exhibit different bandwidths. It is notable that the mode-alignment across channels is also apparent in three cases. A thorough study on the filter bank structure of MVMD and MNCMD is not in the scope of this work and it would be an interesting topic for further investigation.

4.3. Quasi-orthogonality of MNCMD modes

Because the predefined basis function of Fourier-based or wavelet-based methods, such as STFT and WT, are orthogonal, they can ensure there is no information leakage across different modes. However, the data-driven decomposition approaches do not use specific basis function, which enable them to be adaptive but also lead to a problem: is there any information leakage across their modes? Therefore, it is critical to empirically demonstrate the quasi-orthogonality.

In this section, the multiple realizations of 4-channel wGn process, which is adopted to reveal the filer bank structure in the previous section, are used to test the quasi-orthogonality of MNCMD's modes. Herein, the correlation coefficient (44) is used as a measure to quantify the dependence between mode i and j: [1].

$$\rho_{i,j} = \frac{\mathrm{cov}\left(g_i, g_j\right)}{std(g_i) \times std\left(g_j\right)} \tag{44}$$

where $\mathrm{cov}(\cdot)$ and $std(\ \cdot\ )$ denote the covariance and standard deviation, respectively. The closer the correlation coefficient is to 0, the better the orthogonality between these two modes. The correlation coefficient matrices for the set of $Q = 8$ modes obtained from MEMD, MVMD, and MNCMD for 4-channels wGn are transformed into gray-scale images, and displayed in Fig. 11. Black and white denote 1 and 0, respectively. It is observed that the correlation coefficient matrix in the case of MNCMD is almost a diagonal structure, indicating a great quasi-orthogonality among MNCMD modes. While the matrices of MEMD and MVMD show some 'leakage' between adjacent modes because their second diagonals show some gray, especially for MEMD. Consequently, it is inferred the proposed MNCMD outperforms MEMD and MVMD in quasi-orthogonality.

4.4. Influence of channel number

Like the previous work [1], 500 realizations of wGn with channel number $M = 2, 4, 8,$ and 16 are generated, and decomposed by MNCMD. For each case, the influence of M on the mode-alignment property, filter bank structure and quasi-orthogonality are investigated. The first and second rows in Fig. 12 display the resulting filter bank plots and correlation coefficient matrices, respectively. It can be seen that the filter bank and mode-alignment properties within MNCMD are not affected by increasing channel number M. Similarly, the diagonal nature of the bottom row of Fig. 12 highlights the quasi-orthogonality of MNCMD is perfectly retained as M is varying.

4.5. Noise robustness

The univariate NCMD is very robust to noise [2]. In theory, the proposed MNCMD inherits the property of NCMD as a result of being a natural multivariate extension. Thereby, MNCMD should have gratifying noise robustness. The related experiments are conducted on the bivariate signal (39). This signal is added with a noise $\eta(t)$, where $\eta(t) \sim \mathcal{N}\left(0, \sigma^2\right)$. Let σ vary from 0 to 1 with interval 0.01. An animation is attached to provide a visual comparison of the decomposition performance between MNCMD and MVMD. Specifically, Fig. 13 (a) and (b) display the decomposition results of MNCMD and MVMD respectively when $\sigma = 1$. It can be

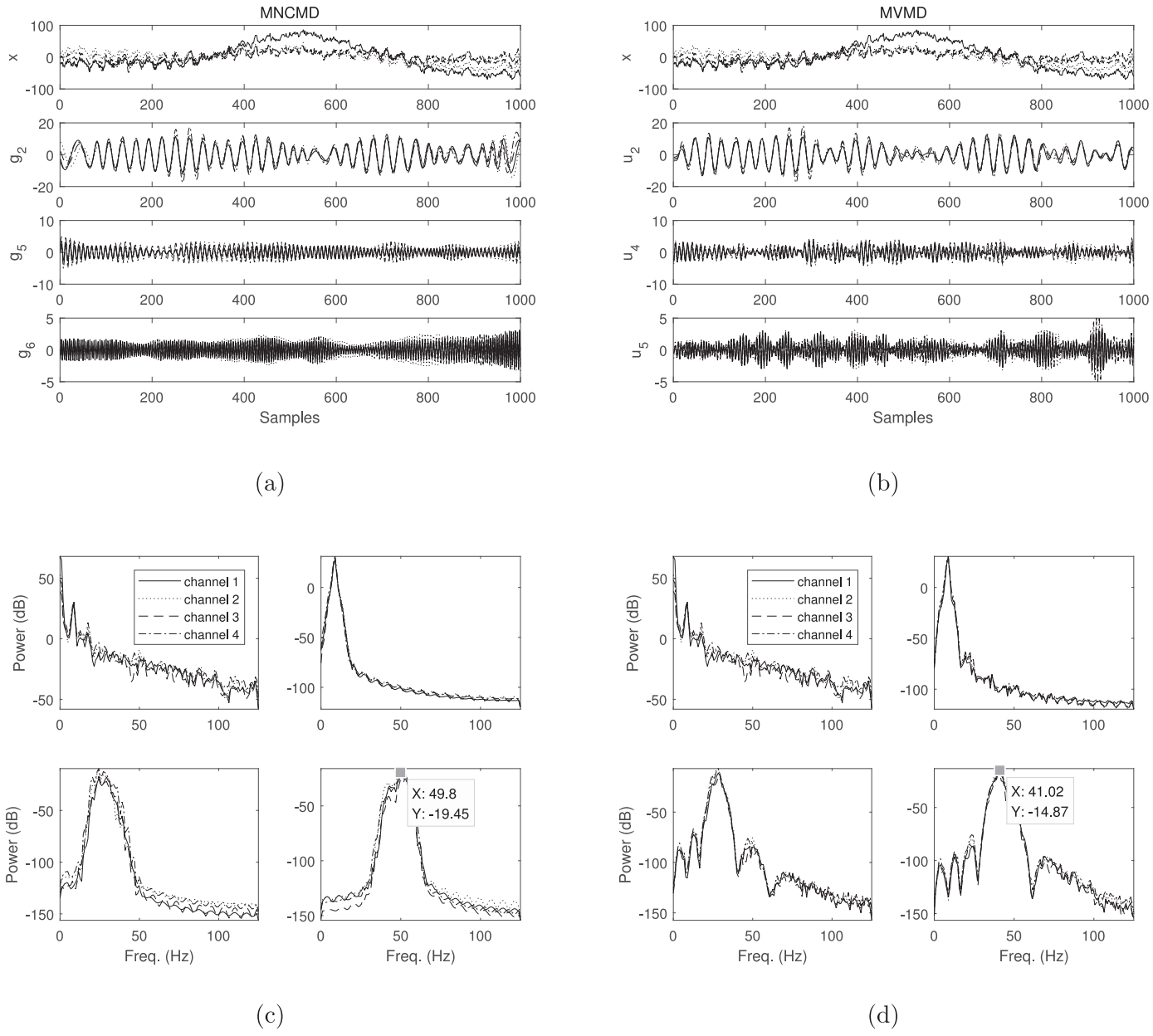

Fig. 16. 4-channel EEG signals and the selected modes obtained by MNCMD and MVMD. (a): Time plots of 4-channel EEG signals and the selected modes (g_2, g_5, g_6) obtained by MNCMD. (b): Time plots of 4-channel EEG signals and the selected modes (u_2, g_4, u_5) obtained by MVMD. (c): Power spectra of the 4-channel EEG signals (top left) and the selected modes (g_2 (top right), g_5 (lower left), g_6 (lower right)) obtained by MNCMD (d): Power spectra of the 4-channel EEG signals and the selected modes (u_2 (top right), u_4 (lower left), u_5 (lower right)) obtained by MVMD.

seen that the MNCMD recovers the common modes of 36-Hz tones in both channels. The 2-Hz and 24-Hz components are presented in $g_{1,1}$ and $g_{2,2}$, respectively. However, for MVMD, although it correctly extracts the 36-Hz signal, the other two tones are fully destroyed. Therefore, it is concluded that the MNCMD has better performance than MVMD in noise robustness. More comparisons are provided in the attached animation.

4.6. Convergence

Although we cannot provide a detailed convergence analysis in the scope of this paper, an experimental investigation on the convergence and sensitivity to initial conditions is conducted [2,13]. Herein, (39) is used as the test subject. In the test, the initial IF consists of two parts: (i) the true instantaneous frequencies IF_t, and (ii) random errors IF_e, namely, $IF_{init} = IF_t + IF_e$. In this case, IF_t of the three modes are 2 Hz, 24 Hz, and 36 Hz, respectively; the corresponding random errors IF_e follow uniform distributions $U(-1,1)$, $U(-5,5)$, and $U(-5,5)$, respectively. A total of 100 random initial instantaneous frequencies are generated. In order to quantify the convergence performance, the following reconstruction error (RE) is used as the measurement.

$$RE = \sum_{i=1}^{Q}\sum_{m=1}^{M} \|g_{i,m} - \tilde{g}_{i,m}\|_2 \tag{45}$$

where $Q = 3$, $M = 2$; $g_{i,m}$ and $\tilde{g}_{i,m}$ are the true modes and extracted modes, respectively. Fig. 14 shows the convergence curves, which indicate MNCMD could converge to satisfactory results.

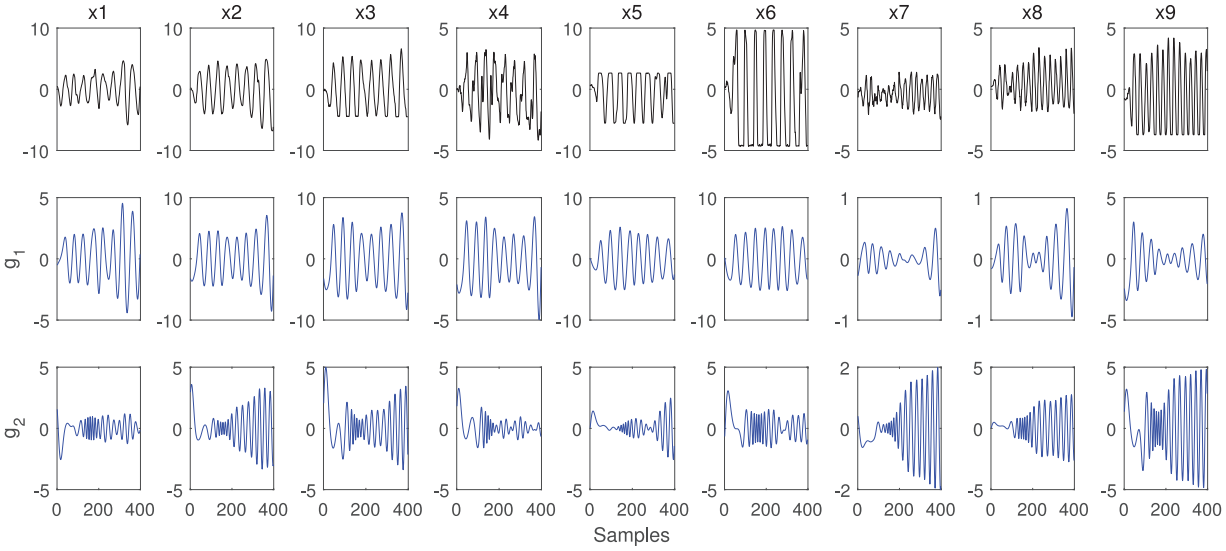

(a)

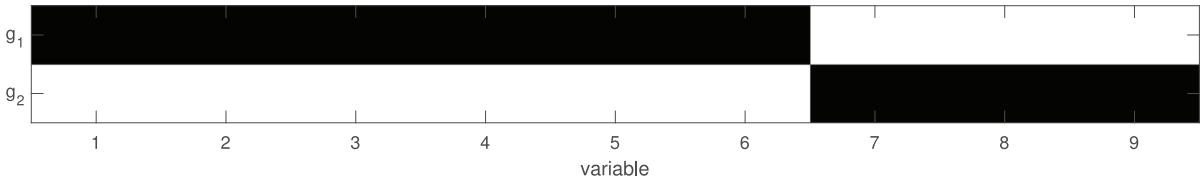

(b)

Fig. 17. (a): The plant-wide oscillations and their decomposition results obtained from MNCMD. (b): The normalized correlation coefficient matrix is transformed into a gray-scale image. The darker the color, the stronger the correlation. Values less than the threshold are set to 0.

5. Real-world applications

Because of the promising performance of MNCMD on simulated signals, more real-world applications can be expected. In order to demonstrate the effectiveness and advantages of the proposed MNCMD in practical applications, herein, three typical examples in various fields are studied, i.e., (i) the analysis of an oceanographic float position record (two-channel), (ii) the separation of α-rhythms in EEG data (four-channel), and the plant-wide oscillation detection in industrial control systems (nine-channel).

5.1. Oceanographic float position records

The first real-world example is taken from the Eastern Basin experiment. It contains position records of a subsurface oceanographic float. The float was deployed in North Atlantic ocean to track the trajectory of salty water flowing the Mediterranean Sea. This data set is available online (http://wfdac.whoi.edu). The input bivariate signal and its 2-D representation are displayed in Fig. 15(a) (top row) and (b) (top left), in which the bivariate oscillations (2-D rotations) are quite apparent [24].

The MNCMD is applied to the bivariate signal with an aim to separate its primary multivariate oscillations. The records are decomposed into 4 modes, as shown in Fig. 15(a) and(b). It is observed that the evident rotations in the original signal have been isolated in separate components. Not all modes are rotating but primarily the last two ones, which correspond to the presumed coherent vortex. The rotating modes can a prior be used to extract finer informations and the non-rotating components may reveals the information about the background fluctuations determining the vortex position [24]. This experiments on the practical data set indicate the ability of MNCDM to effectively separate multivariate oscillations from input signals while also demonstrating the mode-alignment property again.

5.2. Separation of α-rhythms in EEG

The analysis and process of multivariate Electroencephalogram (EEG) signals are always attended for brain computer interface (BCI), which can be used to understand the functional state of brain [20]. Herein, the proposed MNCMD are applied to decompose a 4-channel EEG signal. This data set was sampled from an experiment that involved a subject who kept relaxed and eyes-closed state for a period of time [1]. It is known that α-rhythms are detected in EEG signal during the relaxed state with eyes closed. The frequency range of α-rhythms is $8 - 12$ Hz and the sampling frequency is 250 Hz.

Fig. 16 (a) and (c) display the time-domain waveforms and frequency spectrum of the original signals and selected modes (g_2, g_5, g_6) obtained from MNCMD, respectively. From the graphs above, we can see that the α-rhythm within EEG is localized in mode g_2. It is apparent that all channels corresponding to g_2 contains the same α-rhythm thus emphasizing the mode-alignment property of MNCMD again. The rest modes exhibit the similar mode-

Table 2
Plant-wide oscillation detection results based on MNCMD. (unit: samples per cycle).

mode	x_1	x_2	x_3	x_4	x_5	x_6	x_7	x_8	x_9	actual
g_1	464	458	460	454	452	454	-	-	-	**465**
g_2	-	-	-	-	-	-	258	258	262	**266**

alignment phenomenon, too. As for the performance of MVMD, its corresponding decomposition results are shown in Fig. 16 (a) and (d), which indicate that MVMD captures the α-rhythm in mode u_2 and remain mode-alignment property. It is worth noting that, both g_6 in MNCMD and u_5 in MVMD correspond to artifacts due to the AC mains power line, thus its frequency should be about 50 Hz [1]. However, Fig. 16 (d) (lower right) indicates that the power frequency detected by MVMD is about 40 Hz, which is not in accordance with the fact. By contrast, MNCMD could correctly capture this component, as presented in the lower right of Fig. 16(c). Therefore, MNCMD shows better performance in this case.

5.3. Detection of plant-wide oscillations

The last real-world example is detecting plant-wide oscillations in process control systems. Oscillation is one of the most common abnormal phenomena encountered in process control systems. Although the oscillation is usually generated in one or two loops, it often propagates through the interconnected loops so that it causes plant-wide oscillations. They can cause plants to be run in suboptimal conditions and may result in the waste of raw materials, increased energy consumption and even compromised stability and safety [14]. Consequently, it is necessary to detect and analyze the plant-wide oscillations before the control problem is resolved via proper service and troubleshooting.

The plant-wide oscillation data are provided by [31], where oscillations in a flotation circuit in a mineral concentrator plant are observed. The sampling time is 10 s. The first row of Fig. 17(a) shows the measurements of 9 variables. The MNCMD decomposition modes (g_1, g_2) are displayed in the rest rows.

Based on the decomposition results, an oscillation detector can be carried out. The normalized correlation coefficient (46) is a common index used to discard the pseudo oscillation modes [14].

$$\zeta_{i,m} = \frac{\rho_{i,m}}{\{\rho_{1,m}, \rho_{2,m}, \dots \rho_{Q,m}\}} \tag{46}$$

where $\rho_{i,m}$ is the correlation coefficient between $g_{i,m}$ and x_m, for $i = 1, 2, \dots, Q$ and $m = 1, 2, \dots, M$. Only the modes with ($\zeta > T_\zeta$) are retained, where the threshold T_ζ is 0.35 empirically. The corresponding normalized correlation coefficient matrix is transformed into gray-scale image and presented in Fig. 17(a). It can be seen that the first modes in $x_1 - x_6$, and the second modes in $x_7 - x_9$ are retained for significant oscillations. Then the oscillation periods are estimated by zero crossings [14] and the results are listed in Table 2. The last column in this table is a prior known oscillation period. It is observed that the estimated oscillation periods obtained from MNCMD is completely consistent with the actual situation [31], i.e. there is a slower common oscillation present in $x_1 - x_6$ and a faster common oscillation in $x_7 - x_9$. Consequently, the proposed MNCMD is able to be applied to detect plant-wide oscillations in process control systems.

6. Conclusions

In this paper, a multivariate nonlinear chirp mode decomposition (MNCMD) algorithm is proposed to decompose multivariate signals into a set of sub-signals. We first extend the univariate NCM to its multivariate form (MNCM), which has a common or joint frequency components across all channels. Then, based on the fact that a time-varying MNCM can be demodulated into a multivariate narrow-band signal, an optimal demodulation problem is established. The objective function aims to minimize the sum of bandwidths of all modes across all channels. Minimization of this function is efficiently achieved thorough ADMM. Apart from inheriting the desired characteristics of NCMD, this multivariate extension can extract an optimal set of multivariate modes and their corresponding instantaneous frequencies without requiring more user-defined parameters than the univariate NCMD.

Compared with other multivariate signal decomposition methods, such as MVMD and MEMD, the proposed MNCMD has been shown to exhibit great superiorities on a variety of properties, including mode-alignment, filter bank structure, quasi-orthogonality, robustness to channel number and noise level. Specifically, the proposed MNCMD has at least fourfold advantages:

(i) MNCMD remains mode-alignment property for time-varying multivariate signals; while MVMD is unable to process such signals, thus lacks this property in these cases;

(ii) MNCMD could provide time-frequency information contained in the input data; while MVMD is formulated in the frequency domain, and thus it cannot display such information.

(iii) The modes of MNCMD have better quasi-orthogonality than those of MVMD and MEMD, which means MNCMD has less information 'leakage' across different modes;

(iv) MNCMD is more robust to noise than MVMD and MEMD.

In the end, we highlight the utility and advantages of the proposed method in three typical real-world applications.

Declaration of interests

The authors declare that they have no known competing financial interests or personal relationships that could have appeared to influence the work reported in this paper.

CRediT authorship contribution statement

Qiming Chen: Conceptualization, Methodology, Software, Writing - original draft. **Lei Xie:** Supervision, Writing - review & editing, Visualization. **Hongye Su:** Supervision, Data curation, Validation.

Acknowledgments

The authors would like to thank the sponsors from National Key R&D Program of China (No. 2018YFB1701102), Natural Science Foundation of Zhejiang, China under grand No. LR17F030002, Science Fund for Creative Research Groups of the National Natural Science Foundation of China (Grant No. 61621002).

Appendix A. Proof on the equivalence of (22) and (23)

Note that (23) is the scaled form of augmented Lagrangian function (22) [40]. By combining the linear and quadratic terms in (22) and scaling the dual variable, the related computation would be more convenient. Herein, we will prove they are equivalent.

Proof:

For (22), defining $R_m = \boldsymbol{\omega}_m + \sum_{i=1}^{Q}\left(\boldsymbol{A}_i\boldsymbol{u}_{i,m} + \boldsymbol{B}_i\boldsymbol{v}_{i,m}\right) - \boldsymbol{x}_m$, we have

$$\begin{aligned}
&\sum_{m=1}^{M}\boldsymbol{\lambda}_m^T\left(\boldsymbol{\omega}_m + \sum_{i=1}^{Q}\left(\boldsymbol{A}_i\boldsymbol{u}_{i,m} + \boldsymbol{B}_i\boldsymbol{v}_{i,m}\right) - \boldsymbol{x}_m\right)\\
&\quad + \sum_{m=1}^{M}\frac{\alpha}{2}\left\|\boldsymbol{\omega}_m + \sum_{i=1}^{Q}\left(\boldsymbol{A}_i\boldsymbol{u}_{i,m} + \boldsymbol{B}_i\boldsymbol{v}_{i,m}\right) - \boldsymbol{x}_m\right\|_2^2\\
&= \sum_{m=1}^{M}\boldsymbol{\lambda}_m^T R_m + \sum_{m=1}^{M}\frac{\alpha}{2}\|R_m\|_2^2. \qquad (A.1)
\end{aligned}$$

Firstly, we consider the case with only one channel, namely, $M = 1$,

$$\begin{aligned}
&\sum_{m=1}^{M}\lambda_m^T R_m + \sum_{m=1}^{M}\frac{\alpha}{2}\|R_m\|_2^2 = \lambda_1^T R_1 + \frac{\alpha}{2}\|R_1\|_2^2 = \frac{\alpha}{2}\left\|R_1 + \frac{1}{\alpha}\lambda_1\right\|_2^2\\
&\quad - \frac{1}{2\alpha}\|\lambda_1\|_2^2. \qquad (A.2)
\end{aligned}$$

When $M > 1$

$$\begin{aligned}
&\sum_{m=1}^{M}\boldsymbol{\lambda}_m^T R_m + \sum_{m=1}^{M}\frac{\alpha}{2}\|R_m\|_2^2\\
&= \boldsymbol{\lambda}_1^T R_1 + \frac{\alpha}{2}\|R_1\|_2^2 + \ldots + \boldsymbol{\lambda}_M^T R_M + \frac{\alpha}{2}\|R_M\|_2^2\\
&= \frac{\alpha}{2}\left\|R_1 + \frac{1}{\alpha}\boldsymbol{\lambda}_1\right\|_2^2 - \frac{1}{2\alpha}\|\boldsymbol{\lambda}_1\|_2^2 + \ldots + \frac{\alpha}{2}\left\|R_M + \frac{1}{\alpha}\boldsymbol{\lambda}_M\right\|_2^2\\
&\quad - \frac{1}{2\alpha}\|\boldsymbol{\lambda}_M\|_2^2\\
&= \sum_{m=1}^{M}\left(\frac{\alpha}{2}\left\|R_m + \frac{1}{\alpha}\boldsymbol{\lambda}_m\right\|_2^2 - \frac{1}{2\alpha}\|\boldsymbol{\lambda}_m\|_2^2\right)\\
&= \sum_{m=1}^{M}\left(\frac{\alpha}{2}\left\|\boldsymbol{\omega}_m + \sum_{i=1}^{Q}\left(\boldsymbol{A}_i\boldsymbol{u}_{i,m} + \boldsymbol{B}_i\boldsymbol{v}_{i,m}\right) - \boldsymbol{x}_m + \frac{1}{\alpha}\boldsymbol{\lambda}_m\right\|_2^2\right.\\
&\quad \left. - \frac{1}{2\alpha}\|\boldsymbol{\lambda}_m\|_2^2\right). \qquad (A.3)
\end{aligned}$$

Therefore,

$$\begin{aligned}
&\sum_{m=1}^{M}\lambda_m^T\left(\omega_m + \sum_{i=1}^{Q}\left(\mathbf{A}_i\mathbf{u}_{i,m} + \mathbf{B}_i\mathbf{v}_{i,m}\right) - \mathbf{x}_m\right)\\
&\quad + \sum_{m=1}^{M}\frac{\alpha}{2}\left\|\omega_m + \sum_{i=1}^{Q}\left(\mathbf{A}_i\mathbf{u}_{i,m} + \mathbf{B}_i\mathbf{v}_{i,m}\right) - \mathbf{x}_m\right\|_2^2\\
&= \sum_{m=1}^{M}\left(\frac{\alpha}{2}\left\|\omega_m + \sum_{i=1}^{Q}\left(\mathbf{A}_i\mathbf{u}_{i,m} + \mathbf{B}_i\mathbf{v}_{i,m}\right) - \mathbf{x}_m + \frac{1}{\alpha}\lambda_m\right\|_2^2\right.\\
&\quad \left. - \frac{1}{2\alpha}\|\lambda_m\|_2^2\right) \qquad (A.4)
\end{aligned}$$

Namely, (22) is equivalent to (23).
Q.E.D.

Appendix B. Discussion on frequency calculation of MNCMD and MVMD

In the proposed MNCMD, the instantaneous frequency updates from multiple number of channels are *power-weighted* average to estimate a single estimate of instantaneous frequency [36], shown as

$$\boldsymbol{f}_i^{k+1}(t_n) = \frac{\sum_{m=1}^{M}\boldsymbol{f}_{i,m}^{k+1}(t_n)\left|\boldsymbol{a}_{i,m}^{k+1}(t_n)\right|^2}{\sum_{m=1}^{M}\left|\boldsymbol{a}_{i,m}^{k+1}(t_n)\right|^2} \qquad (B.1)$$

where $\boldsymbol{a}_{i,m}^{k+1}(t_n)$ is the instantaneous amplitude at time t_n and $\left|\boldsymbol{a}_{i,m}^{k+1}(t_n)\right|^2$ represents the power and is the weighting factor. (B.1) has the same form as in [36] and is consistent with the joint instantaneous frequency. Specifically, if a channel does not have a certain frequency component, the amplitude of the corresponding frequency will be 0, which would not interfere with the instantaneous frequency calculation of this layer. This idea (B.1) is not fabricated out of thin air, but inspired by the central frequency updating formula of MVMD [1]

$$\omega_i^{k+1} = \frac{\sum_m\int_0^\infty \omega\left|\hat{u}_{i,m}(\omega)\right|^2 d\omega}{\sum_m\int_0^\infty\left|\hat{u}_{i,m}(\omega)\right|^2 d\omega} \qquad (B.2)$$

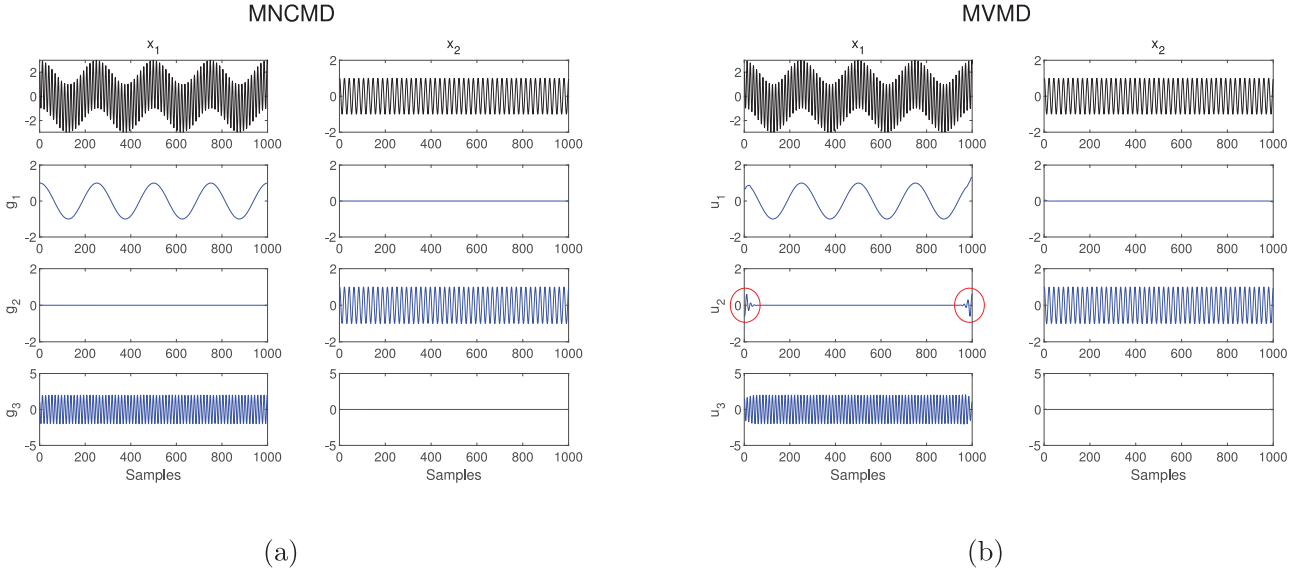

Fig. B.1. MNCMD (a) and MVMD (b) decomposition results in case where there are contrasting set of profiles from individual channels. It is observed that both methods could process such signals, which indicates the power-weighted average framework is reasonable and effective.

where ω is the frequency; $\hat{u}_{i,m}(\omega)$ is the Fourier transform of mode $u_{i,m}(t)$; $\left|\hat{u}_{i,m}(\omega)\right|^2$ is the square of the amplitude corresponding to the frequency ω and it is the weighting factor; ω_i is the center frequency of the ith mode. Clearly, (B.2) indicates MVMD updates the center frequency by taking the contributions from power spectrum of all channels into account, namely, the center frequency of each channel is weighted and averaged according to its power. This is a very promising view. Inspired by Parseval theorem, the weighted average operation in the frequency domain can be performed in the time domain equivalently. As a result, (B.1) is naturally established.

Both (B.1) and (B.2) aim at using multichannel frequency information to estimate single channel frequency information. The difference is that (B.2) is in the frequency domain, while (B.1) is in the time domain. Also, it can be found that (B.2) can only show the information of the whole spectrum, thus MVMD cannot provide time domain information; while MNCMD can reveal these information. When the instantaneous frequencies are constant, the performance of MNCMD and MVMD would be similar (shown in Section 4.1.1).

Herein, (B.3) is tested to demonstrate the weighted average framework can deal with cases where there are contrasting set of profiles from individual channels.

$$\begin{cases} x_1(t) = \cos(2\pi 2t) + 2\cos(2\pi 36t + \pi/3) \\ x_2(t) = \cos(2\pi 24t) \end{cases} \tag{B.3}$$

where $x_1(t)$ contains two tones with 2 Hz and 36 Hz, respectively; $x_2(t)$ only has one 24 Hz component. Namely, there are no common frequency components between channels. The corresponding decomposition results of MNCMD and MVMD are displayed in Fig. B.1(a) and (b), respectively. It is observed that both methods can process such signals well, which indicates the power-weighted average framework is reasonable and effective.

Supplementary material

Supplementary material associated with this article can be found, in the online version, at doi:10.1016/j.sigpro.2020.107667.

References

[1] N. ur Rehman, H. Aftab, Multivariate variational mode decomposition, IEEE Trans. Signal Process. 67 (23) (2019) 6039–6052.
[2] S. Chen, X. Dong, Z. Peng, W. Zhang, G. Meng, Nonlinear chirp mode decomposition: a variational method, IEEE Trans. Signal Process. 65 (22) (2017) 6024–6037.
[3] D. Gabor, Theory of communication. part 1: the analysis of information, J. Inst. Electr. Eng.-Part III 93 (26) (1946) 429–441.
[4] L. Cohen, Generalized phase-space distribution functions, J. Math. Phys. 7 (5) (1966) 781–786.
[5] I. Daubechies, The wavelet transform, time-frequency localization and signal analysis, IEEE Trans. Inf. Theory 36 (5) (1990) 961–1005.
[6] N.E. Huang, Z. Shen, S.R. Long, M.C. Wu, H.H. Shih, Q. Zheng, N.-C. Yen, C.C. Tung, H.H. Liu, The empirical mode decomposition and the hilbert spectrum for nonlinear and non-stationary time series analysis, Proc. R. Soc. Lond. Ser. A 454 (1971) (1998) 903–995.
[7] Z. Wu, N.E. Huang, Ensemble empirical mode decomposition: a noise-assisted data analysis method, Adv. Adapt. Data Anal. 1 (1) (2009) 1–41.
[8] J.-R. Yeh, J.-S. Shieh, N.E. Huang, Complementary ensemble empirical mode decomposition: a novel noise enhanced data analysis method, Adv. Adapt. Data Anal. 2 (2) (2010) 135–156.
[9] J.S. Smith, The local mean decomposition and its application to EEG perception data, J. R. Soc. Interface 2 (5) (2005) 443–454.
[10] M.G. Frei, I. Osorio, Intrinsic time-scale decomposition: time–frequency–energy analysis and real-time filtering of non-stationary signals, Proc. R. Soc. A 463 (2078) (2006) 321–342.
[11] I. Daubechies, J. Lu, H.-T. Wu, Synchrosqueezed wavelet transforms: an empirical mode decomposition-like tool, Appl. Comput. Harmon. Anal. 30 (2) (2011) 243–261.
[12] J. Gilles, Empirical wavelet transform, IEEE Trans. Signal Process. 61 (16) (2013) 3999–4010.
[13] K. Dragomiretskiy, D. Zosso, Variational mode decomposition, IEEE Trans. Signal Process. 62 (3) (2013) 531–544.
[14] Q. Chen, X. Lang, L. Xie, H. Su, Detecting nonlinear oscillations in process control loop based on an improved VMD, IEEE Access 7 (2019) 91446–91462.
[15] Z. Du, X. Chen, H. Zhang, R. Yan, Sparse feature identification based on union of redundant dictionary for wind turbine gearbox fault diagnosis, IEEE Trans. Ind. Electron. 62 (10) (2015) 6594–6605.
[16] T.Y. Hou, Z. Shi, Data-driven time–frequency analysis, Appl. Comput. Harmon. Anal. 35 (2) (2013) 284–308.
[17] Q. Chen, J. Chen, X. Lang, L. Xie, S. Lu, H. Su, Detection and diagnosis of oscillations in process control by fast adaptive chirp mode decomposition, Control Eng. Pract. 97 (2020) 104307.
[18] L. Stanković, M. Brajović, M. Daković, D. Mandic, On the decomposition of multichannel nonstationary multicomponent signals, Signal Process. 167 (2020) 107261.
[19] A. Zahra, N. Kanwal, N. ur Rehman, S. Ehsan, K.D. McDonald-Maier, Seizure detection from EEG signals using multivariate empirical mode decomposition, Comput. Biol. Med. 88 (2017) 132–141.
[20] W. Von Rosenberg, T. Chanwimalueang, V. Goverdovsky, D. Looney, D. Sharp, D.P. Mandic, Smart helmet: wearable multichannel ECG and EEG, IEEE J. Transl. Eng. Health Med. 4 (2016).
[21] H. Hao, H.L. Wang, N.U. Rehman, A joint framework for multivariate signal denoising using multivariate empirical mode decomposition, Signal Process. 135 (2017) 263–273.
[22] L. Stanković, D. Mandić, M. Daković, M. Brajović, Time-frequency decomposition of multivariate multicomponent signals, Signal Process. 142 (2018) 468–479.
[23] T. Tanaka, D.P. Mandic, Complex empirical mode decomposition, IEEE Signal Process. Lett. 14 (2) (2007) 101–104.
[24] G. Rilling, P. Flandrin, P. Gonçalves, J.M. Lilly, Bivariate empirical mode decomposition, IEEE Signal Process. Lett. 14 (12) (2007) 936–939.
[25] N. ur Rehman, D.P. Mandic, Empirical mode decomposition for trivariate signals, IEEE Trans. Signal Process. 58 (3) (2009) 1059–1068.
[26] N. Rehman, D.P. Mandic, Multivariate empirical mode decomposition, Proc. R. Soc. A 466 (2117) (2009) 1291–1302.
[27] N. Rehman, M.M. Khan, M.I. Sohaib, M. Jehanzaib, S. Ehsan, K. McDonald-Maier, Image fusion using multivariate and multidimensional EMD, in: 2014 IEEE International Conference on Image Processing (ICIP), IEEE, 2014, pp. 5112–5116.
[28] X. Lang, D. Zhong, L. Xie, J. Chen, Application of improved multivariate empirical mode decomposition to plant-wide oscillations characterization, in: 2017 6th International Symposium on Advanced Control of Industrial Processes (AdCONIP), IEEE, 2017, pp. 601–606.
[29] X. Lang, Q. Zheng, Z. Zhang, S. Lu, L. Xie, A. Horch, H. Su, Fast multivariate empirical mode decomposition, IEEE Access 6 (2018) 65521–65538.
[30] X. Lang, Z. Zhang, L. Xie, A. Horch, H. Su, Time-frequency analysis of plant-wide oscillations using multivariate intrinsic time-scale decomposition, Ind. Eng. Chem. Res. 57 (3) (2018) 954–966.
[31] X. Lang, Q. Zheng, L. Xie, A. Horch, H. Su, Direct multivariate intrinsic time-scale decomposition for oscillation monitoring, IEEE Trans. Control Syst. Technol. (2019).
[32] A. Ahrabian, D. Looney, L. Stanković, D.P. Mandic, Synchrosqueezing-based time-frequency analysis of multivariate data, Signal Process. 106 (2015) 331–341.
[33] O. Singh, R.K. Sunkaria, An empirical wavelet transform based approach for multivariate data processing application to cardiovascular physiological signals, Bio-Algo. Med-Syst. 14 (4) (2018).
[34] Y. Wang, F. Liu, Z. Jiang, S. He, Q. Mo, Complex variational mode decomposition for signal processing applications, Mech. Syst. Signal Process. 86 (2017) 75–85.
[35] M.-C. Pan, Y.-F. Lin, Further exploration of vold–kalman-filtering order tracking with shaft-speed informationâi: theoretical part, numerical implementation and parameter investigations, Mech. Syst. Signal Process. 20 (5) (2006) 1134–1154.
[36] J.M. Lilly, S.C. Olhede, Analysis of modulated multivariate oscillations, IEEE Trans. Signal Process. 60 (2) (2011) 600–612.
[37] S. Meignen, D.-H. Pham, S. McLaughlin, On demodulation, ridge detection, and synchrosqueezing for multicomponent signals, IEEE Trans. Signal Process. 65 (8) (2017) 2093–2103.
[38] Y. Yang, X. Dong, Z. Peng, W. Zhang, G. Meng, Component extraction for non-stationary multi-component signal using parameterized de-chirping and band–pass filter, IEEE Signal Process. Lett. 22 (9) (2014) 1373–1377.
[39] S. Chen, Y. Yang, K. Wei, X. Dong, Z. Peng, W. Zhang, Time-varying frequency-modulated component extraction based on parameterized demodulation and singular value decomposition, IEEE Trans. Instrum. Meas. 65 (2) (2015) 276–285.
[40] S. Boyd, N. Parikh, E. Chu, B. Peleato, J. Eckstein, et al., Distributed optimization and statistical learning via the alternating direction method of multipliers, Found. Trends® Mach. Learn. 3 (1) (2011) 1–122.
[41] N. Parikh, S. Boyd, et al., Proximal algorithms, Found. Trends® Optim. 1 (3) (2014) 127–239.
[42] B.-K. Park, O. Boric-Lubecke, V.M. Lubecke, Arctangent demodulation with DC offset compensation in quadrature doppler radar receiver systems, IEEE Trans. Microw. Theory Tech. 55 (5) (2007) 1073–1079.

[43] N. Rehman, D. Looney, T.M. Rutkowski, D.P. Mandic, Bivariate EMD-based image fusion, in: 2009 IEEE/SP 15th Workshop on Statistical Signal Processing, IEEE, 2009, pp. 57–60.
[44] N. ur Rehman, B. Khan, K. Naveed, Data-driven multivariate signal denoising using mahalanobis distance, IEEE Signal Process Lett. 26 (9) (2019) 1408–1412.
[45] D. Looney, D.P. Mandic, Multiscale image fusion using complex extensions of EMD, IEEE Trans. Signal Process. 57 (4) (2009) 1626–1630.
[46] N. Ur Rehman, D.P. Mandic, Filter bank property of multivariate empirical mode decomposition, IEEE Trans. Signal Process. 59 (5) (2011) 2421–2426.